universität
wien

DIPLOMARBEIT

Titel der Diplomarbeit

Morphometric shape analysis of the human ear:
Approaches via 3D Surface-scans of plaster mould
models in the determination of sex

>Band 1<

Verfasserin

Katharina Baron

angestrebter akademischer Grad

Magister der Naturwissenschaften (Mag.rer.nat.)

Wien, März 2011

Studienkennzahl lt. Studienblatt: A 442

Studienrichtung lt. Studienblatt: Diplomstudiengang Anthropologie (A442)

Betreuerin / Betreuer: Univ. Prof. Fred L. Bookstein PhD

I

In memoriam of Paul Baron

Eidesstattliche Erklärung

Ich versichere hiermit, diese Arbeit selbständig verfasst zu haben. Des weiteren versichere ich, dass keine anderen als die angegebenen Quellen und Hilfsmittel benutzt wurden, und ich mich auch sonst keiner unerlaubten Hilfsmittel bedient habe.

I assure, that I have written this work independently. Furthermore, I assure that nothing else but the given references and scientific resources have been used, and I have not helped myself of unauthorized aid.

_____

Signature

Acknowledgements

Kurzfassung

Das Potenzial von menschlichen Außenohren für die persönliche Identifizierung wurde erstmals von Alphonse Bertillon im Jahre 1890 beschrieben (Bertillon 1890, zitiert durch Hurley et al., 2000). In den letzten 120 Jahren untersuchten mehrere Studien biometrische Unterschiede bei menschlichen Ohren um spezifische Identifizierungen festzustellen. Dabei wurden unter anderem Zeichnungen, Photographien und 3D Oberflächenscanner-Daten verwendet.

Bezüglich der spezifischen Frage nach einem Geschlechtsunterschied an menschlichen Ohren, wurden von Sforza et al. Im Jahr 2009 vergleichbare geschlechtsspezifische Dimensionen von Ohren analysiert. Die vorliegende Diplomarbeit versucht zu beweisen, dass 3D Oberflächenscans von menschlichen Ohren eine passende Methode für die Analyse von Geschlechtsunterschieden darstellt.

Die zu vergleichende Stichrobe (n=29, 14♂, 15♀; durchschnittliches Alter: 25.3 Jahre) besteht aus 3D Oberflächenscans (David Lasercanner 2.4.3) von Gipsmodellen.

Nachdem 72 Landmarks inklusive 67 Semilandmarks in Amira 5.2.0 gesetzt wurden, wurden diese Punkte in Edgewarp 3.30 zueinander verschoben (sliding). Anschließend wurden die Daten in Morpheus et al. geladen, gruppiert und mit f (weiblich) und m (männlich) bezeichnet und superimposed (GPA) bevor ein MANOVA P-Test durchgeführt wurde. Außerdem wurde ein PCA in R 1.12.1 berechnet.

Die Ergebnisse zeigten, dass es im Bezug auf Geschlechtsunterschiede keine bedeutenden Unterschiede gibt (Versetzungstest / randomized Beispiel 999: p=0.384). Aus den ersten beiden Hauptkomponenten der Analyse ergaben sich eine erklärte Varianz von 44.47% im s.g. shape space und 43.66% im s.g. form space. Von den 29 Proben insgesamt sechs aus der Studie ausgeschlossen, da diese Mängel in den Oberflächendaten aufwiesen. Aufgrund dieser heruntergesetzten Stichprobe ist es leider nicht eindeutig möglich einen klaren Geschlechtsunterschied auszumachen. Die Verwendung der Gipsabdrücke zeigte allerdings eine sehr hohe Genauigkeit im Bezug auf die Morphometrie des Ohres. In Bezugnahme auf den David Laserscanner zeigte sich, dass eine maximaler Fehler von 3mm pro Scan erwartet werden könnte, da dieser von vielen verschiedenen Hardware-Komponenten abhängig ist.

Generell lässt sich sagen, dass das Potenzial des David Laserscanner 2.4.3 für die Analyse von komplexen Strukturen wie menschlichen Ohren begrenzt ist.

Abstract

The potential of human external ears for personal identification was first recognized and described by Alphonse Bertillon in 1890 (Bertillon 1890, cited by Hurley et al. 2000). In the last 120 years several studies investigated biometric differences in human ear shape for specific identification using drawings, photographs and 3D surface scan data.

Including the question of sexual dimorphism, Sforza et al. (2009) described sex-related dimensions of ears. This diploma thesis tried to verify that 3D surface scans of human ears are an appropriate method for the analysis of sexual dimorphism, which could then be used in biometric recognition systems, as well as in standard craniofacial development, human evolution or diseases.

My comparative sample (Caucasians, n=29, 14♂, 15♀;average age: 25.3 years) consists of 3D surface scans of plaster mould models from living volunteers. After scanning, 72 landmarks including 67 semilandmarks were set with Amira 5.2.0 and were slid in Edgewarp 3.30. Afterwards, after loading the data in Morpheus et al. they were grouped, labeled with f (female) and m (male), and superimposed (GPA) before performing MANOVA. Furthermore a PCA in R 1.12.1 was calculated.

For this sample there are no significant differences (permutation test/ randomized sample 999: p=0.384) in the determination of sex as well as in the analysis of every single curve.

Including all digitized specimens (11♂, 12♀; Caucasian, age average: 25.4 years), six specimens were excluded due to missing data, 44.47% of the variance is explained by the first two principal components in shape space. Furthermore, 43.66% of the variance is explained in the first two principal components in form space. Analyzing every curve separately shows similar results.

The reduced sample size of 23 specimens does not allow an accurate prediction of sexual dimorphism of human ears. However, the usage of the plaster mould model showed very good accuracy in comparison to the ears' actual geometry. The accuracy of the David Surface scanner 2.4.3 (DAVID Vision Systems GmbH, Germany), depends on various hardware components and settings like the camera distance, the object size, the light conditions, the triangulation angle and the quality of the calibration target. In this study a maximum error of not more than 3mm per scan can be expected, due to the camera distance of 300 mm. In general, it could be shown that there is only a limited potential of the David Laser scanner 2.4.3 (as an example for 3D surface scanners) for the analysis of complex structures like human ears.

Directory

I. Introduction

1. Anatomy, physiology and embryonic developmental biology

This section is a short theoretical background about the anatomy of the human ear, its embryonic development and studies dealing with the external ear structure for sexual dimorphic pattern.

1.1 Anatomy of the human ear

The ear itself can be differentiated into three sections: the external ear, the tympanic cavity and the interior ear , whereas there are two sensory parts, which have different functions, but form one morphological complex (the inner ear). The first part of the inner ear, the cochlea, is the acoustic organ. The second part includes sacculus, utriculus and the semicircular canals, and registers in particular the changes of position of the head as well as the rest of the human body. This part represents the so-called vestibular system (Kahle and Frotscher, 2005).

The border between the external and internal ear structure is set at the beginning of the ear canal.

The visible part, called pinna (see Figure 1) is an organ that can be subdivided into several different parts.

The helix builds the outer edge of the ear; the antihelix builds a hill and forms a Y shape on the upper ear part.

In this region the antihelix splits into superior and

Figure 1: Anatomy of the external ear

inferior cruxes which are building a depression between these Y-shaped structure, the so called fossa triangularis.

Furthermore the tragus and the antitragus (see Figure 1) are visible; right above the tragus lays the anterior crux of the helix and the cymba conchae. The concha builds the deepest depression in the auricle.

Besides the lobule, the auricular (pinna) possesses a skeleton of flexible cartilage. The form of the bulges and hollows differs between every human and are genetically determined. The form of the following anatomical structures is determined by genetics: Helix, antihelix, scapha, concha auriculae, tragus, antitragus and fossa triangularis (Kahle and Frotscher, 2005). The external ear canal is stiffened primarily by flexible cartilage and further on by bone. The skin of the cartilage area contains sebaceous glands and ceruminous glands. These glands are similar to sweat glands, the so called apocrine glands (Lüllmann- Rauch, 2006).
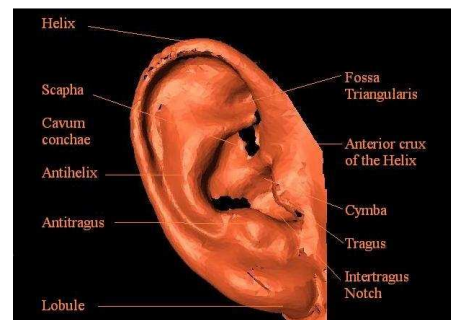
1.2   The development of the human ear, growth and sexually dimorphic pattern

In 1997 Wright described the development of the external ear as a complex process which reaches from the early embryonic stage to the postnatal period. Parallel to the anatomical changes of the pharyngeal arch during the fifth week of gestation, the external ear as well as the auditory ear canal develops. Both of these areas

Figure 2: Embryonic development of the ear

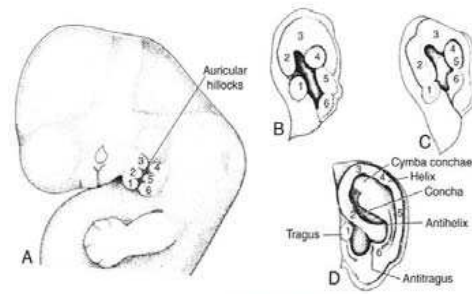develop until the age age of nine, although the ear is already formed by birth. (Wright, 1997)

Six tubercles grow from the mandibular arch as well as the hyoid arch during the sixth week. They are called tragus, crus of the helix, helix, lobule, antitragus and the antihelix (Sadler and Langman, 2003). During the second and third month of development the pinna (external ear structure) expresses its form (see Figure 2).

The ear is built of one plate of fibro-cartilage which is covered by the skin and is connected with the circumjacent parts by extrinsic muscles and ligaments and fibrous fabrics (Foucar, 1940). This thin plate produces the helix (the curved edge of the ear) and furthermore the antihelix (counterpart of the helix) (Foucar, 1940).

Besides the development of the outer ear structure and the growing pattern of ears, some important morphometrical studies on the ear anatomy were performed to determine sexual dimorphic pattern, and will be explained further to give a short background about morphometrical studies of the external ear.

Peeples et al. (1985) put out, that three of the vertical and the three horizontal measurements seem "*to be under specific genetic regulation*" in both sexes: *"(…) width of the superior helix, distance from superior helix to the edge of antihelix, distance from antihelix to tip of the lobule, (…) width of the pinna, width of the posterior helix, and width of the notch (…)" (Peeples et al., 1985).*

In 2009 Sforza et al. described sex-related dimensions of ears. 497 male and 346 female healthy subjects aged between 4 and 73 years were digitized. Several soft-tissue landmarks were set on the ear and face. The authors concluded, that "*All ear dimensions were larger in men than in women. The ear width-to-length ratio and the sagittal angle of the auricle decreased (…), but without sex related differences. (…) Asymmetry was found in the sagittal*

angle of the auricle (both sexes), in the ear width-to-length ratio and ear width (men only)."(Sforza et al., 2009)

Meijerman et al. (2007) described a cross-sectional anthropometric study to analyze the growth of the outer ear structure to provide a way of predicting which anatomical features appearing in ear prints may vary during lifetime. They analyzed 1353 subjects considering the effects of age on auricle length, earlobe length, and auricle width. However, the antihelix prominence and helix width seemed to be unaffected by age.

In 2007 Niemitz et al. examined 1448 ears from newborn children up to 92 years old adults for growth and sexual dimorphic pattern. They found several sexual dimorphic patterns, whereas male ears showed more increase in growth than those of females. The greatest ear length in male subjects was 52 mm (SD +/- 4.1 mm) at birth, 65 mm (SD +/- 4.0 mm) at around 20 years and 78 mm (SD +/- 4.8 mm) at around 70. For women the results were: 52 mm (SD +/- 4.3 mm), 61 mm (SD +/- 3.9 mm) and 72 mm (SD +/- 4.6 mm) (Niemitz, 2007).

Moreover, Purkait and Singh (2008) described a bilateral comparison of ear patterns in the same individual, where no ear was found to be exactly the same in morphology to its counterpart (right and left ear).

2.   Biometric identification and geometric morphometrics

This section is going to give a review of the usage of human ears for personal identification as well as a basic theoretical background of geometric morphometrics for better understanding the methods used in this study. The following section also gives a short introduction to define the terms of curves and outlines, landmarks and semilandmarks, as well as the procrustes superimposition, ridges and perpendiculars on the turning point of a cubical parabolic three dimensional surface, as a constructed parabolic curvature.

2.1   Personal identification using biometric differences in human ear shape

The potential of human external ears for personal identification was first recognized and described by Bertillon in 1890 (Bertillon 1890, cited by Hurley et al. 2000). In the last 120 years several studies investigated biometric differences in human ear shape for specific identification using drawings, photographs and 3D surface scan data.

The classification work of Iannarelli (1989) was a novel approach in the biometrics of human ears from photographs (see Figure 3). In total over 10000 photographs of human ears from a random sample in California were compared. Burge and Burger (1998) concluded that, if the centre point was set improperly, researchers were faced with the problem that all measurements were incorrect. Additionally, localizing of the anatomical points was not very suitable for automated machine vision. (Hurley, 2007)
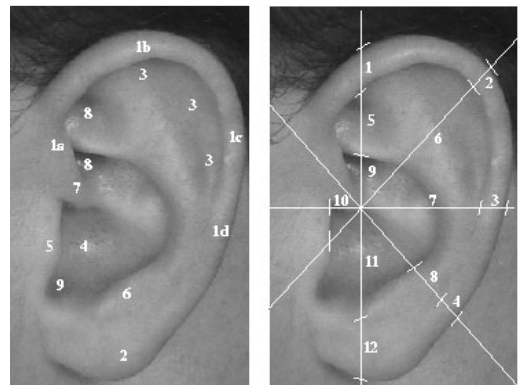
Figure 3: Left: Anatomy, Right: Measurements, (a) 1 Helix Rim, 2 Lobule, 3 Antihelix, 4 Concha, 5 Tragus, 6 Antitragus, 7 Cruz of Helix, 8 Triangular Fossa, 9 Incisure Intertragica. (b) The locations of the anthropometric measurements used in the "Iannarelli System". (Burge et al., 1998)

Moreno et al. (1999) combined the results of 168 photographs using attributes of outer ear points, ear shape information and features extracted by compression network simulating a new identification method.

Burge and Burger (1998 & 2000) used the Voronoi diagram (after Dirichlet 1850) for computing automated biometrics of ear curve segments. They used an algorithm, which takes

4

the possibility of error curves into account. These error curves can be caused by e.g. exposure, light arrangement, shadowing and occlusion.

In the last decade researchers have focused on the general appearance and shape of the human ear, whether using PCA (Victor et al. 2002), force field (Hurley et al. 2000) or ICP (Yan und Bowyer 2004 & 2005).

The so-called 'force field transformation'*("(…)the force field can also be defined directly with its own set of equations (…)"*(Hurley, 2005)*)* for ear recognition was examined by Hurley et al. (2000) by transforming the images as a classification of Gaussian attractors, acting as the sources of a force field. According to the authors this technique provided good results for their research questions.

Studies by Victor et al. (2002) analyzed the comparison between the recognition of the ear and face, by using principal component analysis (PCA) (see Figure 4). (Hurley, 2007)

Additionally, Hurley et al. (2000) used PCA on a subset of 252 ear images extracted from the XM2VTS multi model face profiles database (Messer et al., 1999; Jain, 2007) to achieve a recognition rate of 98.4% in 3D (Hurley, 2007).
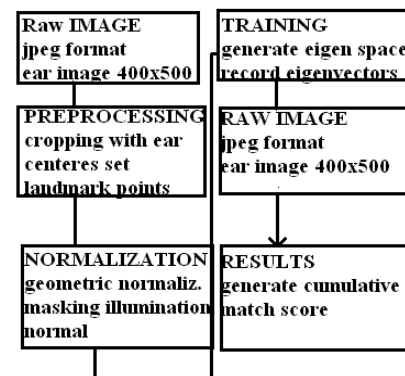

Figure 4: Theoretically methods (Victor et al. 2002)

In 2004 & 2005, Chen and Bhanu used a 'surface shape descriptor' to analyse a 3D ear recognition method. Ten Individual were digitized using two ranged images for each person.

However, the 3D structure of the auricle is only ascertainable only with difficulty, so a handful of research groups have focused on the field of 3D Ear Biometrics. Yan and Bowyer (2004 & 2005) used a Minolta VIVID 910 range scanner to scan the ear via laser technology. By using triangulation algorithms the depth is calculated. (Hurley, 2007) Iterated closest point (ICP) based matching was applied for developing a fully automatic ear biometric system. Disturbing objects from 3D depth data, e.g. earrings, jewellery and hairs, can be easily removed automatically in the 2D model. (Hurley et al., 2007**;** Yan and Bowyer, 2005a/b/c; Yan and Bowyer, 2004 & 2005)

So ICP can be used due to its simplicity and accuracy (Hurley et al., 2007). In 2005b, Yan et al. developed an efficient ICP registration method (precomputed voxel closest neighbours) used for biometric studies of previously processed human ears.

In 2003 Bhanu and Chen used a two-step ICP algorithm. They examined 30 subjects with 3D ear images. Two of 30 individual were found wrong. They build an ear model template from

20 subjects. Besides, Hurley (2007) considered the importance of investigation of specific ear parts from the recognition perspective. Many steps have been taken in the potential means of human ears in personal identification using modern biometrics and morphometrics (Arbab-Zavar, 2007).

Sexual dimorphism could be used in conjunction with biometric recognition systems in several ways. Also Ear morphometrics could be useful for the study of craniofacial development, human evolution, diseases or the biometrics.

2.2 Geometric morphometrics

"Geometric morphometrics is a collection of approaches for the multivariate statistical analysis of Cartesian coordinate data, usually (but not always) limited to landmark point locations. The multivariate part of geometric morphometrics is usually carried out in a linear tangent space to the non-Euclidean shape space in the vicinity of the mean shape." (Slice et al., 1995)

Among others, Pearson (Pearson, 1895) and Fisher (1918 & 1921) developed statistics in the context of biologic-morphological variations, which build the foundation for actual morphometrics. Additionally, statistical methods like principal component analysis (Hotteling, 1933; Pearson, 1901) and the correlation coefficient (Pearson, 1895) were developed. Distances became the most familiar variables used for morphometric measurements methods. These early studies provided many statistical methods, which today allow analysis of more than one variable at the same time.

In 1917, Thompson published constructed deformation grids to show how one part of an individual looks like as a distortion of the same part in another organism (Cartesian transformation (see Figure 5)).

While Thompson had drawn this by hand, Bookstein (1989) introduced the thin plate spline interpolation. This method shows shape differences between two forms as deformations. The new form results out of minimized bending energy (Bookstein, 1997;
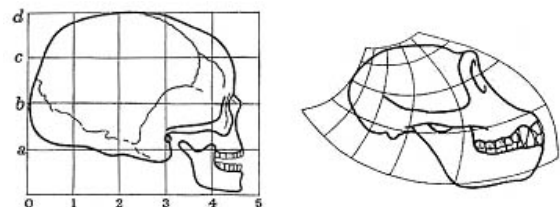
Figure 5: Cartesian transformations (Thompson 1917)

Bookstein et al., 2002; Bookstein et al., 2003; Mitteroecker et al., 2004 and Bastir et al., 2006).

Geometric morphometrics has been developed to analyze form variations by using mathematical points (curves and landmarks) in multidimensional space.

Landmarks were defined in three subtypes and Semilandmarks were introduced with the aim to use *"Landmarks for description of structures that lack true landmarks"* (Bookstein 1991; Bookstein, 1997; Bookstein et al., 1999). Recently, semilandmarks have been used in several morphological studies (Mitteroecker et al., 2004; Mitteroecker et al., 2005; Sheets et al., 2004; Gunz et al., 2005).

The exact knowledge of specific definitions and terminology in the analysis of morphological differences in biological objects is essential to understand the methods of modern geometric morphometrics and will be an important part during this thesis.

Procrustes Superimposition

A system of shape coordinates, consisting of the coordinates of several landmarks after the objects are translated, rescaled and rotated. Therefore first landmark is fixed at the origin and the second landmark is fixed at (1,0) in a cartesian coordinate system. This function is called the Two- point shape coordinate (Bookstein, 1991) (see Figure 6).

Today, extract shape variables from a set of landmarks are called the 'procrustes superimposition'. This method superimposes configurations without using position, orientation and scale of the data (Adams, Rohlf and Slice, 2004).
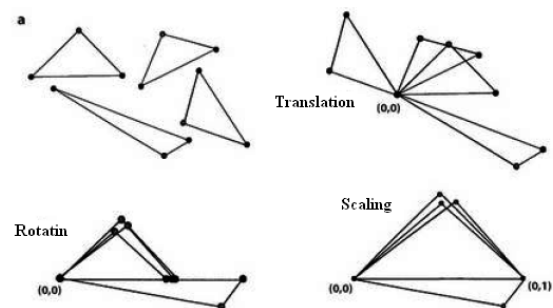
Figure 6: Shape coordinates (after Bookstein 1991)

Therefore, three steps are used, based on the Euclidean similarity transformation (shown in Figure 7) (Dryden and Mardia, 1998).

1. Translate: Translation of the objects. The result should share the same centroid.

2. Scaling: Scaling of the objects. The result should share the same centroid size.

3. Rotation: The object is going to be rotated (minimizing the sum of the squared Euclidian distances.

The generalized procrustes analysis was developed if there are more than two specimens (Gower, 1975; Rohlf and Slice, 1990). The rotation step changes to a specific algorithm. The result of this scaled, centered and rotated landmarks are the procrustes shape coordinats.
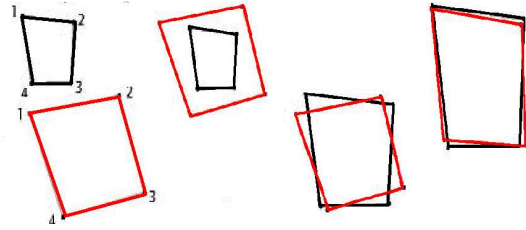

Figure 7: Procrustes superimposition

Landmarks

"Landmarks are the points at which one´s explanation of biological processes are grounded" (Bookstein, 1991).

Landmarks must be homologous between two different forms. Bookstein (1991) stated that landmarks are all defined by specific names (to insure homology) as well as coordinates. In this case homology has to be seen as a function, relating points rather than parts (Bookstein, 1991).

In general, Bookstein (1991) described three types of landmark points:

Type I: Mathematical point who are defined by discrete juxtaposition of tissues, like the correspondence to homologies anatomical structures

Type II: Point of a maximum curvature

Type III: Characterize more than one region of the form, so called extreme points

In 2004 Bookstein and Schaefer and in 2007 Katina et al. described a new landmark classification.

Type I: discrete juxtaposition of tissues

Type II: Point of a maximum curvature

Type III: Characterize more than one region of the form, by using the information of multiple curves and through symmetry.

Type IV: Semilandmarks on ridge Curves. The term of semilandmarks will be explained above (Semilandmarks: landmark-based analysis of outlines see p.9).

Type V: Semilandmarks on surfaces

Type VI: Constructed semilandmarks

Semilandmarks: landmark-based analysis of outlines

"Sliding landmarks make it possible to include outline information in the geometric morphometric analysis." (EVAN 2010)

Sliding of the landmarks is applied to minimize the effects of the random location of semilandmarks along curves (Bookstein, 1996; Bookstein, 1997; Bookstein et al., 2002; Gunz et al., 2005).

The aim of this technique is to slide points along the external curve until they correspond optimally to their equivalents in the right configuration and consequently serve the principles of procrustes superimposition (Bookstein, 1997).

To minimize the procrustes distance (Rohlf, 1998) or the bending energy (Bookstein, 1997; Bookstein et al., 2002; Bookstein et al., 2003; Mitteroecker et al., 2004 and Bastir et al., 2006) semilandmarks can be slid along tangents defined by other semilandmarks.

Outlines

The aspect of analysing an object can include outlines which are closed or open. Closed, means the starting and endpoint are the same – comparable to the outline of a circle; open means the starting and endpoint are different like a curved line. Here the starting and endpoint is clear. For simplification of analysis, a series of points along the outline are marked first, otherwise the decision of which variable on the line should be analysed is quite complex. Depending on the analysis method the starting point can be recorded at every specimen and is correspondent or not (Klingenberg, 2009)**.** There are multiple ways of analyzing an outline.

Eigenshape analysis

"Any region that can be defined as a closed curve can be subjected to a standard eigenshape analysis."(McLeod, 1999 p.4)

In general the digitization for the standard eigenshape analysis starts at a landmark point along a curve of a margin (Lohmann, 1983; Lohmann and Schweitzer 1990b). If specimens lack common landmarks, they can be analyzed using a so-called generalized superimposition method (Lohmann, 1983). When using the generalized superimposition method the digitization of the starting point fits to a specific location. The location is determined including the corresponding part of the outline or the outline within shape space (McLeod, 1999). Using a landmark as starting point is a common procedure and has been published several times (Kucera and Malmgren, 1996; Lohmann and Schweitzer ,1990a and 1990b; MacLeod and Rose, 1993; MacLeod and Carr, 1987; Norris et al., 1996; Ray, 1990; Lohmann and Schweitzer, 1990; Norris et al., 1996).

Curves along extreme points: Ridges

Ridges are lines which are running along extreme points (for example parabolics) (see Fig. 8 red). These lines or curves are building a perpendicular curvature along the maximum points along the perpendicular direction (Weber & Bookstein 2011).

Perpendicular lines along the turning points of a cubic parabolic surface

Cubic parabolic curvatures are polynomial equations of the third degree. In general, the function is defined by the following equation: $y = f(x) = a*x^3 + b*x^2 + c*x + d$ including $a \neq 0$ (see Figure 8) (Lauter et al., 2000)

Setting a perpendicular line as a reconstructed parabolic curve along the turning points of a cubic parabolic surface can also be demonstrated in a three-dimensional grid, shown in Figure 9 (green line) (Koenderink, 1990).
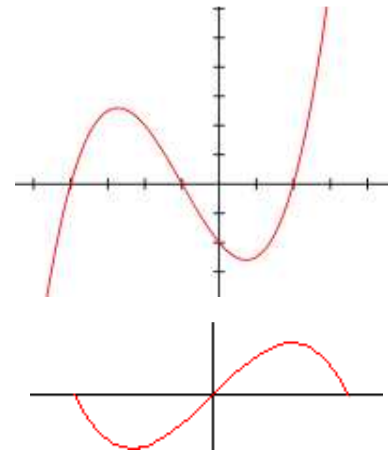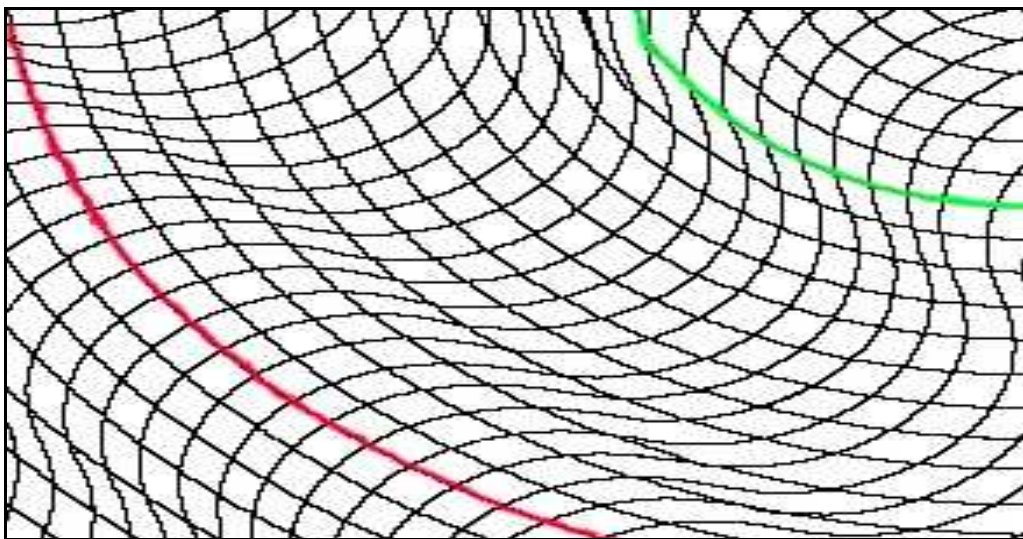

Figure: 8: polynomial of the third degree

Figure 9: rigdes(red); perpendicular curve alonge the turning points of cubic parabolic (green)

3. Technical Background

This section is going to give a detailed technical background of the methods used in this study. Special attention is drawn to the setting and calibration of the used surface scanner to facilitate future scientific studies performed with the David Laser scanner 2.4.3.

3.1 Modelling with Alginat

Alginate is normally used in dentistry for dental elastic impressions and provides results in good medical qualities. It is free of additives like fiberglass shavings, is dust free, has a fine pasty consistence and is extremely precise. The product used in this study was Kromopan 100 idrocolloide, Lascod S.p.A- Laboratori scientific odonoiatria. The volume ratio for impressions like ears is one part of Alginate to 1.5 parts of water, including a processing time of nearly 90 seconds.

3.2 Contact-free active and passive scanning

Active scanner capture objects by detecting theirs reflection, by using radiations like laser light or light (Weber & Bookstein 2011). In comparison to a passive scanner, active systems are more sensitive to surface properties (Lanman and Taubin, 2009).
An example for contact-free active scanner would be the David Laser scanner 2.4.3 (David Surface scanner 2.4.3, DAVID Vision Systems GmbH, Germany) used in this study. This scanner system uses a vertical laser light line to process the object.

Passive scanner does not need to use radiations (specific light sources) itself, but detect reflected surrounding radiations to build an image (Weber and Bookstein 2011).

3.3 David Laser scanner 2.4.3 (David Surface scanner 2.4.3, DAVID Vision Systems GmbH, Germany)

The David Laser scanner consists of a standard consumer digital camera (webcam) and a hand held line-scanner (Class 1 laser). Two plain boards in the background form the calibration plate panel situated in an 90 degree angle to each other, a desktop PC and the DAVID-Laser scanner software (DAVID 3D Scanner: Jan 2011).

3.3.1 Camera Calibration

Before starting scanning, the camera has to be calibrated because the system establishes the orientation and position of the camera in the three Dimensional space as well as its parameters like lens and focus length (DAVID 3D Scanner: Jan 2011).

To obtain optimal scans, the scanner should be connected to the PC, before choosing the camera device and the image format. The camera has to be placed in front of the camera corner like in Figure 10, so all calibration plate patterns fill the camera image. To calibrate the camera right, a minimum number of six points at the panel have to be visible as well a high contrast should be appointed. Also important is to choose the right scale for the calibration pattern.
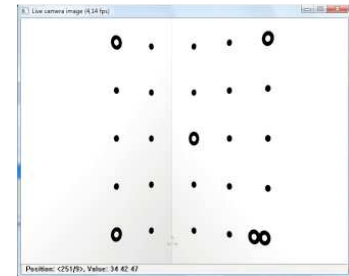

Figure 10: Camera Calibration corner (David Laser scanner 2.6.0

After pressing the "Calibrate Camera" button there should be red crosses on the black pattern, than the calibration is complete.

3.3.2 Scanning Process

The object should be placed between the camera and the calibration corner (see Figure 11). It should be centred in the middle of the camera image, be in focus and the camera settings (exposure time, aperture) should be adjusted.

Figure 11: Live Camera Image

Adjust the camera settings like exposure time and aperture. After switching the laser on, the light conditions in the room should not change anymore, the laser line should be clearly visible and bright while the rest of the image should be black. Switch off the laser and press START than switch on the laser, and scan the object. In the scan result image it is possible to control, which regions are already, scanned (see Figure 12).
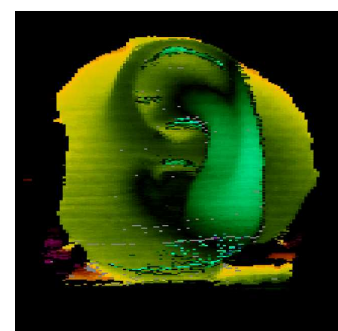
To see the object in 3D you can press "Show 3D" and a 3D-window appears in the software panel, for getting a better result it is possible to take a picture from the texture which is going to be overlaid with the scan (DAVID 3D Scanner: Jan 2011).

Figure 12: Scan result image

3.3.3   Shape Fusion

This software-function combines and aligns all scanned 3D scans. Following steps have to be considered: After adding the entire scan into the input list, the scans can be arranged and then aligned. Therefore, click on the first scan and afterwards on the second scan. After the software shows the two pop-ups "Coarse registration, please wait a few seconds" and "Fine registration, please wait a few seconds" the alignment is completed (see Figure 13).
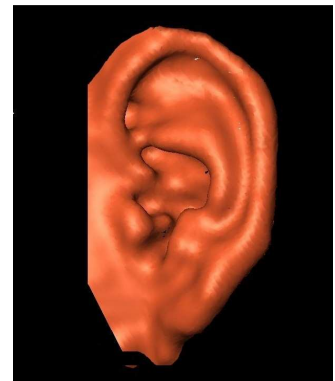

Figure 13: Resulting shape fusion of 10 single scans

4. Hypothesis

The main aim of this study includes the novel aspect of sex specific differences in ear shape, considering morphometric and multivariate analysis methods and statistics as well as 3D surface scanning of outer ear structures.

In contrast to previous studies by Peeples et al. (1985), Meijermann et al. (2007), Niemitz et al. (2007) and Sforza et al. (2009), this study uses the novel approach of 3D surface scanning technique combined with geometric morphometrics to analyse sex specific differences of human ears.

Therefore, this study is concerned with the following hypothesis:

3D surface scans of human ears are an appropriate method for the analysis of sexual dimorphism, which can be used in biometric recognition systems, as well as craniofacial development, human evolution or diseases.

The three main aims of this study can be summarized in the following questions:

1. Are there any sex specific differences in the determination of sexual dimorphism of human ears analyzing 3D image data from the David Laser scanner 2.4.3 with geometric morphometrics?

2. How does a 3D surface scan match the ears actual geometry?

3. What is the potential of the David Laser scanner 2.4.3 (as an example for 3D surface scanners) for the analysis of complex structures?

II.   Material and methods

1   Scanning process

The comparative sample (Caucasians, n=29, 14♂, 15♀; age average: 25.3 years) consists of 3D surface scans (David Surface scanner 2.4.3, DAVID Vision Systems GmbH, Germany) of plaster mould models from living volunteers.

After the standard calibration of the David Laserscanner 2.4.3 (DAVID Vision Systems GmbH, Germany) at the Department of Anthropology (University of Vienna, Austria) a series of test scans of the models were performed to evaluate the best settings. Afterwards, all cast were scanned including following settings (see Table 1. p.22) using a class one 650nm Laser (DIN EN 60825-1:2008-5 /EN 60825-1:2007), a 2-Megapixel-Webcam (1600-1200/ Autofocus Logitech Quickcam 9000 Pro) with a distance of 300mm to the object and the Software DAVID Laserscanner Professional Edition (DAVID Vision Systems GmbH, Germany) as well as using a triangulation angle of approximately 35°.

2   Moulding and cast models

Pretests showed that taking scans of living individuals is going to cause problems during the data analysis. Therefore, 3D cast models were produced. The negative form was made with alginate (Kromopan idrocolloide 100 hour) which was afterwards filled with cast.

Before getting started every test person had to sign an informed consent (see Appendix).

First, the probands got an ear plug before a die was placed around the ear. Further alginate got stirred with the volume ratio of 1 part of Alginate to 1.5 parts of water, resulting a processing time of nearly 1.5 minutes. This mixture was filled in the mold so a negative cast of the ear was formed. After this cast was finished, within 20 minutes the negative form was filled with plaster.

3   3D-Data acquisition and digitizing

The resulting image data were transferred to the software package of the David Laserscanner 2.4.3 (DAVID Vision Systems GmbH, Germany) at the Department of Anthropology, (University of Vienna, Austria) for shape fusion and 3D reconstruction (*.obj).

After transferring all *.obj Files into *.stl Files with MeshLab v1.2.1 (Istituto di Scienza e Tecnologie dell'Informazione/ Stable Developer: Callieri, Corsini, Dellepiane, Ganovelli, Pietroni, Tarini, since 2007), Visage Imaging Amira 5.2.0 (Visage Imaging Inc., San Diego, USA) at the Department of Oral Surgery, Medical University of Vienna, Austria was used for digitizing 72 landmarks including 67 semilandmarks. In total, 23 specimens (11♂, 15♀;

Caucasian, age average: 25.4 years) were included in the study, six (3♂, 3♀) specimens were excluded from the study due to incomplete data in the 3D surfaces.

All landmarks were set along specific curves of the surface structure, four of the curves were open and one of them closed (Figure 16-20)

3.1 Digitizing fixed landmarks

The following chapters explain where on each ear the landmarks were set. Additionally, the digitizing of ridges and perpendiculars on the turning point of a cubical parabolic three dimensional surfaces as constructed parabolic curvatures is shown.

The Figures 14 - 20 are structured as followed: In the left part of the picture an overview of the digitized ear is shown, whereas in the right part two equivalent cross sections are visualized (upper part: orientation in the room; lower part: cross section as example of the set of landmarks).

Landmark point one (ldk1) was set as an extreme point in form of the lowest part between the helix and end of the inferior part of the crux of the antihelix (see Figure 14). Equally to the first landmark, landmark point two (ldk2) was set. This point is positioned on the highest point of the end of the anterior crux of the helix (see Figure 15).

Landmark point three (ldk3) and five (ldk5) were equally set to the first landmark. Landmark point three builds the lowest point between the second and fifth curvature (see Figure 17 and 20), while Landmark point five (ldk5) builds an increase between the antihelix and the antitragus.

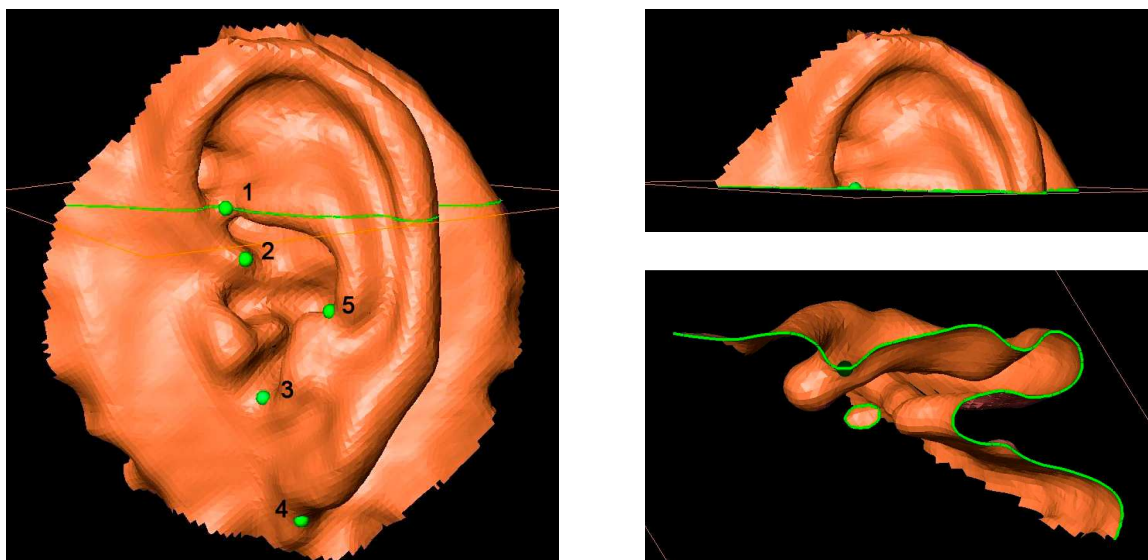Furthermore, the fourth landmark point (ldk4) builds the connection point between the head and the ear lobule.

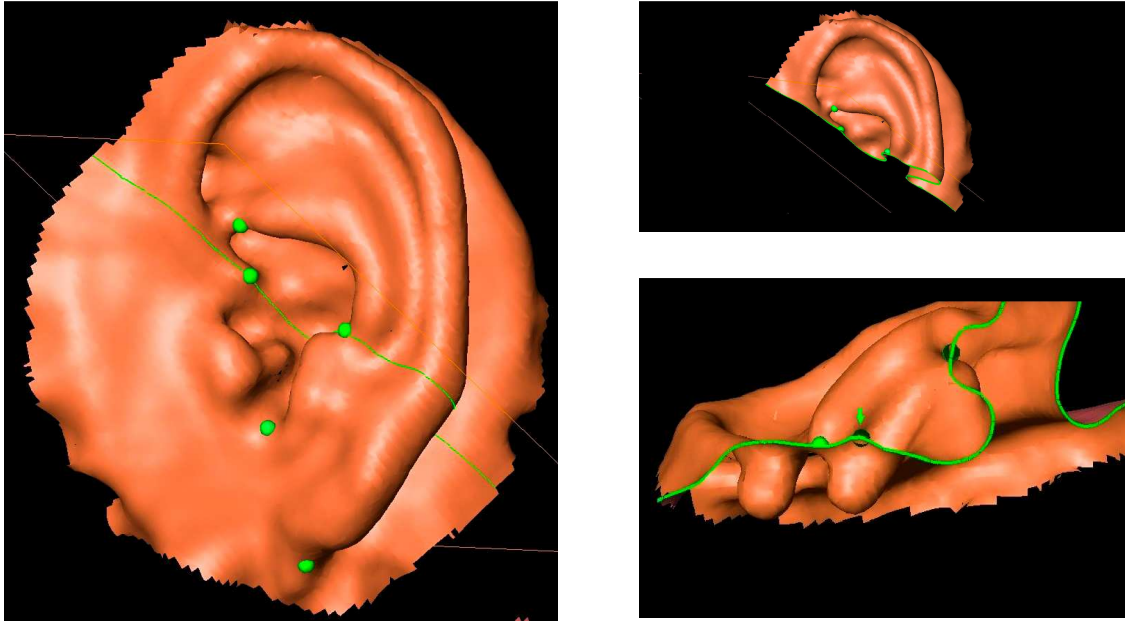**Figure 14:** ldk1 including cross section

Figure 15: ldk2 including cross section

3.2 Digitizing semilandmarks along curves

Every picture on the left side, visualizes every curve separately including the fixed landmarks (shown in blue), while on the right side two cross sections are shown. The upper right pictures show the orientation in the room. The lower right pictures show a cross section, as an example of the set semilandmarks on the current curve. The numbers given in brackets are the equivalent numbers of the semilandmarks later used in the statistical and geometric-morphometrical analysis. The cross section should give a better understanding on which principles curves were found as constructed parabolic- or ridge curves.
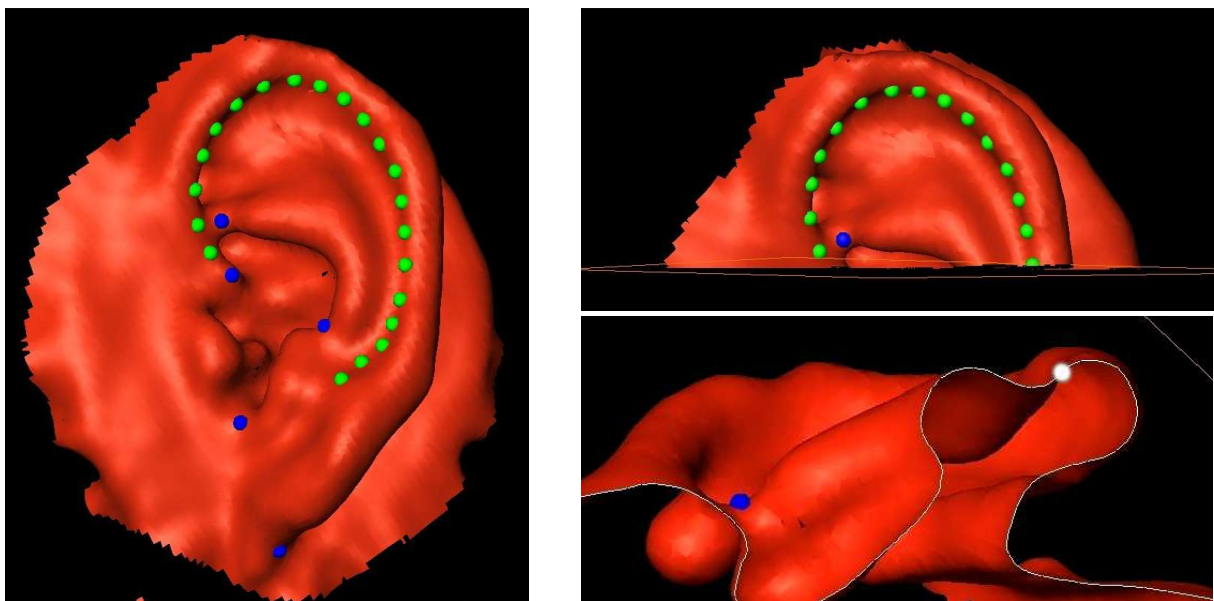

Figure 16: Curve 1 including crosssection

The first curve starts at ldk2 and ends as an open curve, this curve runs along the inner line of the helix (0-24) in form of a perpendicular on the turning point of a cubical parabolic surface (see Figure 16). It's a matter of a constructed parabolic curvature.

The second curve starts at ldk3, runs along the antitragus and ends at ldk5 (25-29). From this region the third curve starts open along the antihelix across the anterior crus of the antihelix and ends at ldk1 (30-38). Curve two and three are both characterized as ridge curves (see Figure 17 and 18)
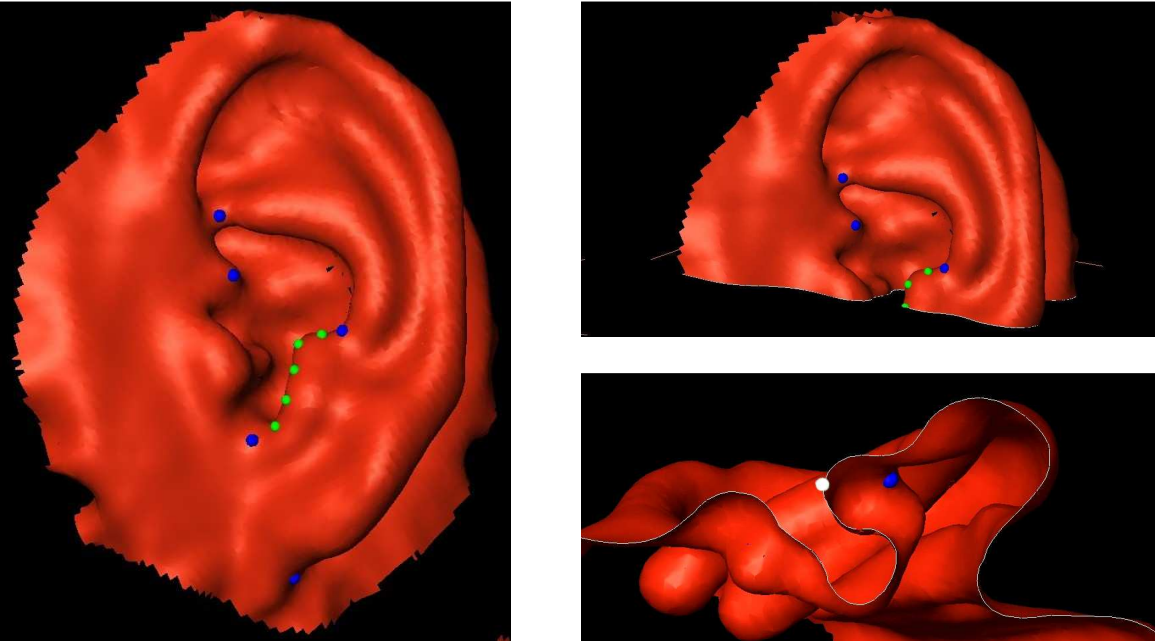

Figure 17: Curve 2 including cross sections
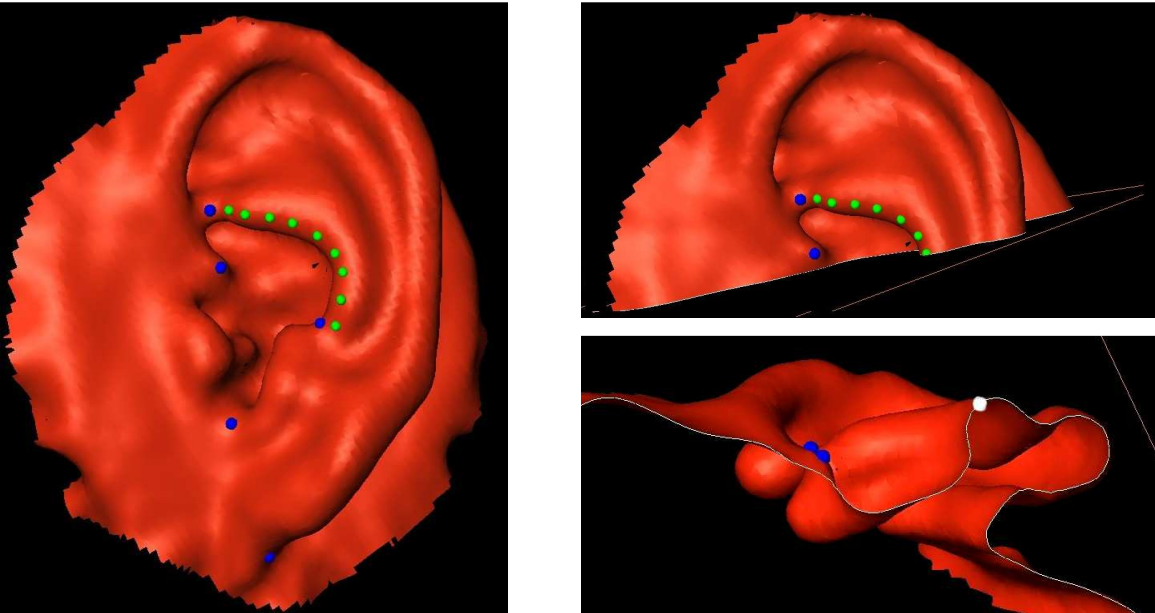

Figure 18: Curve 3 including cross sections

The fourth curve starts at ldk4, the connecting point between the lobule and the head and runs along the outer part of the helix and ends open (39-57). This curve is characterized as a constructed ridge curve (see Figure 19).
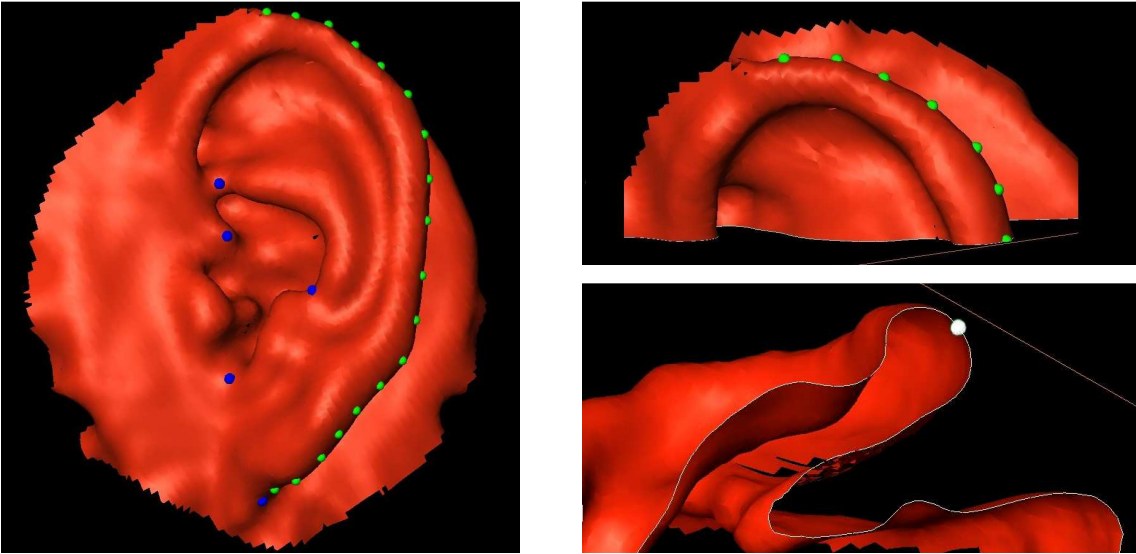

Figure 19: Curve 4 including cross-sections

The fifth curve starts open, runs along the tragus and ends at ldk3 (58-66) (see Figure 20). Each of these semilandmarks runs along a curve, characterized as a ridge curve.
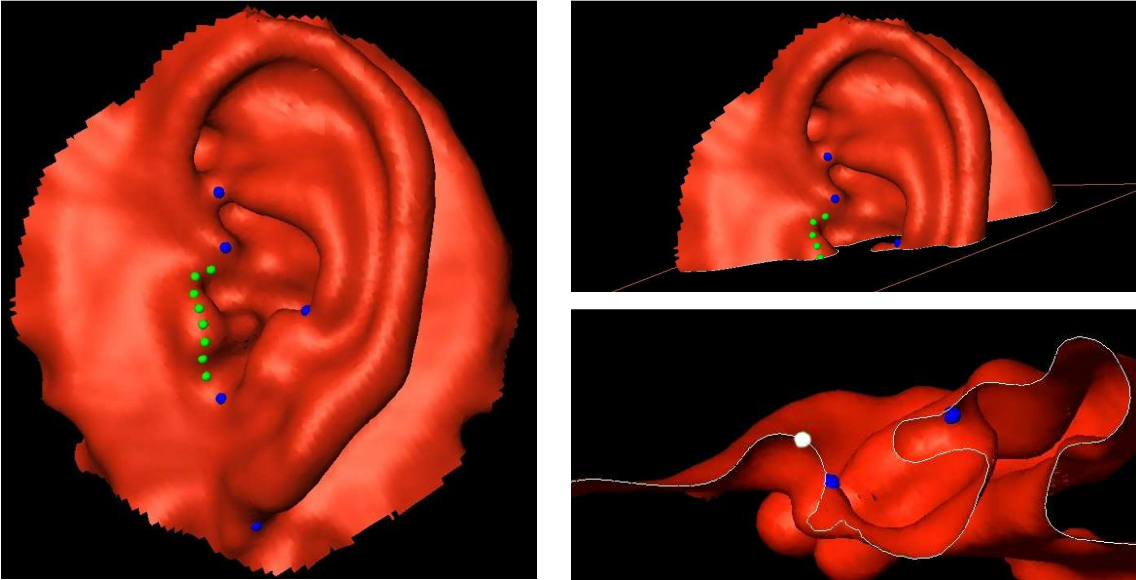

Figure 20: Curve 5 including cross sections

All landmarks were set manually and saved in two different files (fixed LM and Snakes).

3.3 Building the Template and sliding of the semilandmarks

The first set of landmarks was used for building a template.

The template builds the standardized specific file type including following parts:

{	
volume {	
}	
lhs {	= left-hand side, including all landmarks including the slider
}	
rhs {	= right-hand side, in the template file Homogeneous to the lhs
}	
relax {	= gives the exact number of LM (full, full, full) and the exact number of Sliders (none, none, none)
}	
labels {	= gives the exact number of LM (ldk1, ldk2) and the exact number of Sliders (CLcurve1, CLcurve2, CLcurve3)
}	
reference {	
−4.938901801006559e+00 −4.358347213228504e+00 3.970797363729849e+00	
1.201701846531854e+02	
1.000000000000000e+00 0.000000000000000e+00 0.000000000000000e+00	
0.000000000000000e+00 9.999994440794628e−01 1.054438601955762e−03	
0.000000000000000e+00 −1.054438601955762e−03 9.999994440794628e−01	
}	
slice {	
−6.722274374494985e+00 2.850509156010931e+00 −8.731814909854572e+00	
1.333973665077005e+02	
−6.955618819295073e−02 1.374874453434360e−02 −9.974832874328234e−01	
9.950895653789300e−01 −6.962601056071592e−02 −7.034895541065303e−02	
−7.041799172113461e−02 −9.974784161459980e−01 −8.838312329500364e−03	
}	
view {	
−5.451208051530203e−02 1.293508898336573e−01 −6.933366231769916e−02	
1.061617219366657e−02	
−7.449752453455576e−01 6.477135244675469e−01 −1.596216590696746e−01	
6.581740004079645e−01 7.526591479982108e−01 −1.764063835534843e−02	
1.087146218744420e−01 −1.182006647884720e−01 −9.870206349586924e−01 }}	

After the landmarks were set in Amira 5.2.0 (Visage Imaging Inc., San Diego, USA) at the Department of Oral Surgery (Medical University of Vienna, Austria) the data of the landmark-File (5-LM) were exchanged with the LM-data in the rhs-part of the template-file and saved as new *.sav-File (specific specimen). Afterwards, the Snake-File (slider) was transferred into a transcur-file and the segments of the single curves denoted as well as the label named. This part is builds the ground structure of a curve file.

Furthermore the *.obj surface files were converted in Linux OS with the Obj2sur file to *.sur-file formats, so that the program Edgewarp3.30 (Bookstein and Green, 2006) can read the surfaces. It happend that the resulting *.obj surfaces, included degenerated triangles with a 0 point area, which had to be removed first. The so incurred files (*.sav, *.cur and *.sur) were loaded into Edgewarp3.30 (Bookstein and Green, 2006).

Later on, a curve-file was preprocessed and automatically saved as *.curp-file, where all semilandmarks were projected to its curves.

```
ew>moving semi-landmarks ⋯ 67 moved, average 8.3.5, maximum 25
```

Afterwards all semilandmarks were oriented and relaxed until the bending energy change was almost zero by repeating both commands.

```
Setting semi-landmarks direction ⋯ 67 moved, energy change 3,45E¯14, moved average 1,43,
maximum 6.87
```

All sliding points were moved along its tangents until the energy changes between two corresponding points were as small as possible. After this operation the points were projected from the tangent back to its curve.

4   Geometric morphometric analysis including statistics

From the resulting written records of all the *.sav files (which moved the SLM along tangents and projected them back on the curve), the new written rhs coordinates (moved and projected LM) were copied into a single *.txt file (ordered by groups).

After loading the new data (*.txt) in Morpheus et al.(1998) the data was grouped and labeled in f (female) and m (male) and superimposed (GPA) before performing a p-test MANOVA (provides nonparametric, randomization testing for group mean differences).

Furthermore, a PCA in R 1.12.1 (R-Project, Institute of Mathemathics, School of Economics Vienna, 2010) was calculated as well as the data warped in Amira 5.2.0 (Visage Imaging Inc., San Diego, USA) at the Department of Oral Surgery (Medical University of Vienna, Austria). Every single curve was examined and the statistical analysis repeated.

In a further step outliers where excluded and the single curve examination repeated.

**Table 1: Test setting for each Individual**

Individuum		Setting						
Sex	Proband	Calibration plate	Image Formate	Brightness	Contrast	white balance	Expsure time	Sensitivity
F	1							7333
F	2							7334
F	3							7334
F	4							7333
F	5							7334
F	6							7334
F	7							7332
F	8							7333
F	9							7333
F	10							7333
F	11							7333
F	12							7333
F	13							7333
F	14		640x480px 20fps 24bit 24RGB					7332
F	15	50.00		2708	2157	8923	1/250 (s)	7333
M	16							7332
M	17							7333
M	18							7333
M	19							7333
M	20							7334
M	21							7333
M	22							7334
M	23							7334
M	24							7333
M	25							7333
M	26							7334
M	27							7333
M	28							7333
M	29							7333

|	View and save results			Merge Scans/Fuse triangle mesh:				
Sex	Interpolation	Smooth average	smooth median	Resolution	Smoothing	Removel	Methode	Alignment
F	2	3	2		2	2		
F	1	2	2		3	2		
F	2	3	2		3	4		
F	1	2	2		2	2		
F	1	2	2		2	3		
F	2	2	2		3	3		
F	1	3	2		2	3		
F	2	2	2		3	2		
F	2	3	2		2	4		
F	2	2	2		2	2		
F	2	2	3		2	4		
F	2	2	2		3	3		
F	2	3	2		3	1		
F	2	2	2		3	1		
F	2	4	2	150	2	5	simple	Auto
M	2	2	2		3	1		
M	2	2	2		4	2		
M	2	3	2		3	2		
M	2	3	2		2	2		
M	1	2	2		2	3		
M	2	1	2		3	2		
M	2	2	2		2	2		
M	2	1	2		2	3		
M	2	2	2		4	2		
M	2	2	2		3	2		
M	2	1	2		2	1		
M	1	2	1		2	2		
M	2	3	2		3	1		
M	1	2	2		1	1		

III.   Results

1   Separate analysis of every Curve

Every single curve was analyzed separately. Following plots show the first against the second PC in shape as well as in form space separated by Curve 1-5.
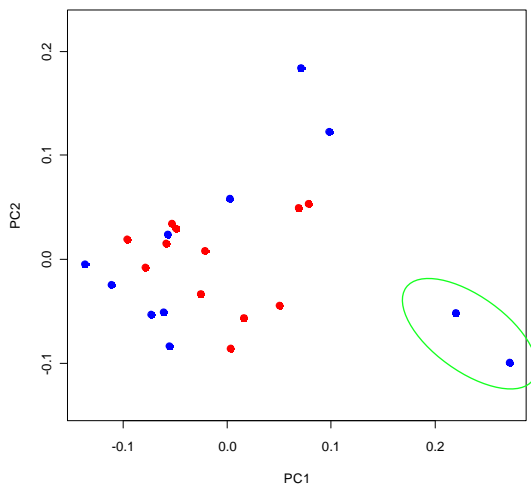
Curve 1
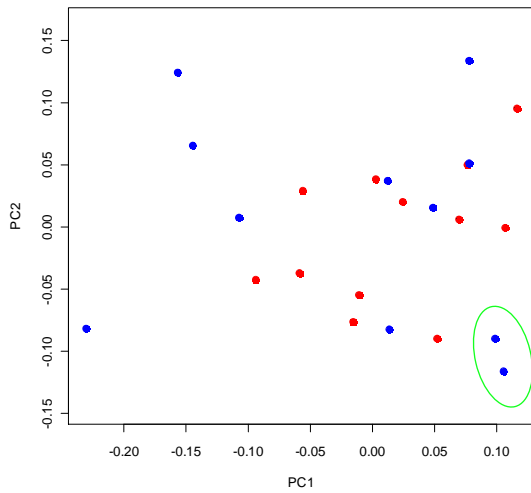
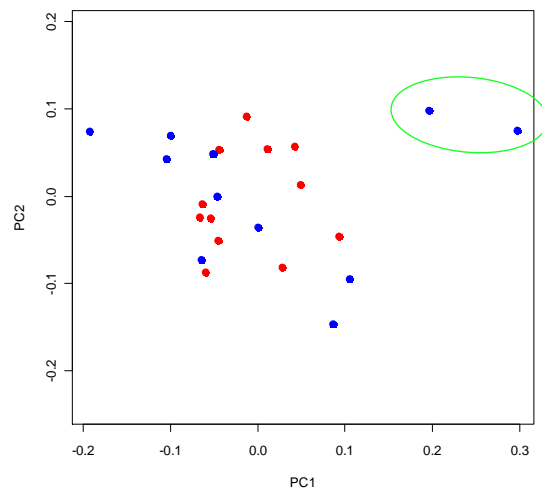**Plot 1**: PC1 against PC2 in shape space (Red=f /Blue=m/ green=marked outlier) for Curve 1
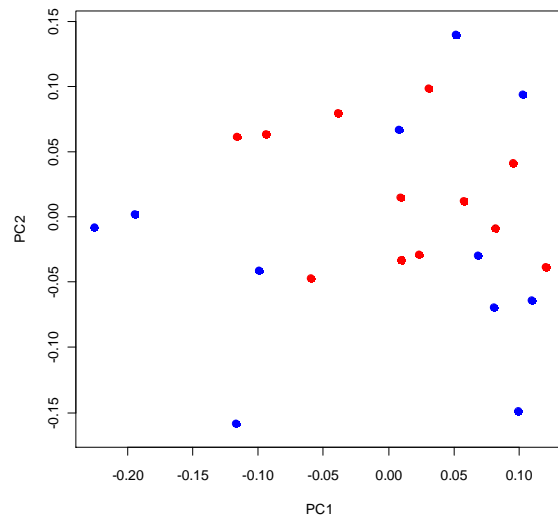
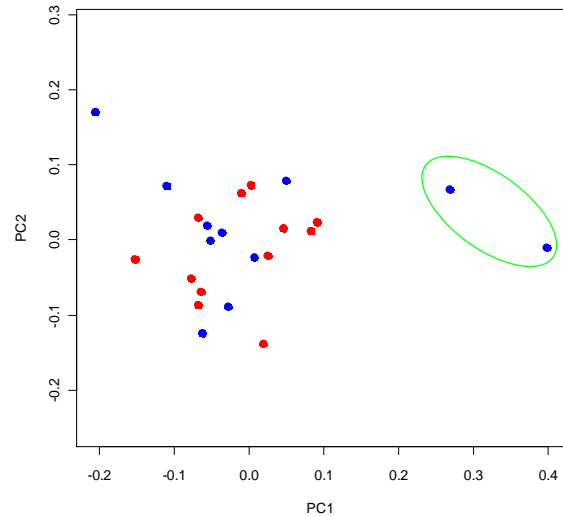**Plot 2:** PC1 against PC2 in form space (Red=f /Blue=m) for curve 1

Curve 2

Plot 3: PC1 against PC2 in shape space (Red=f /Blue=m/ green=marked outlier) for Curve 2

Plot 4: PC1 against PC2 in form space (Red=f /Blue=m/ green=marked outlier) for curve 2

The first two plots show 33.6% and 18.7% of the variance for Curve 1 is explained by the first two partial components in shape space and 30.7% and 18.1% of the variance is explained in the first two partial components in form space. The mean differences in the parabolic curve one are not significant (p=0.379)

Including all specimens 43.5% and 19.6% of the variance for Curve 2 is explained by the first two partial components in shape space and 39.8% and 16.9% of the variance is explained in the first two partial components in form space. (Plot 3, 4) The mean differences in Curve 2 are not significant (p=0.612).
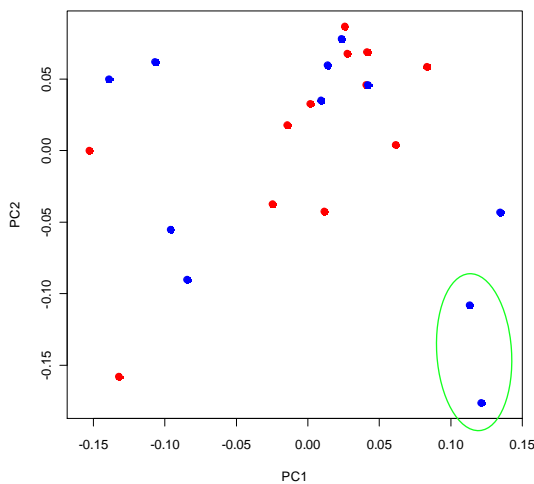
Curve 3
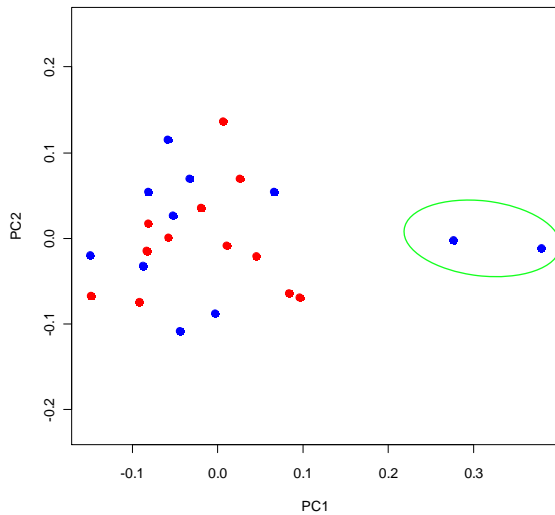
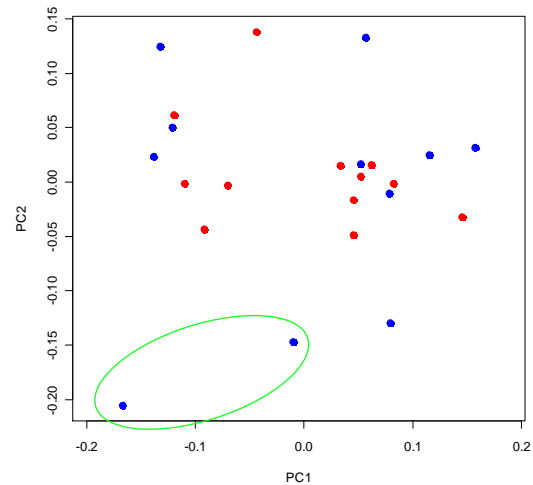**Plot 5**: PC1 against PC2 in shape space (Red=f /Blue=m/ green=marked outlier) for Curve 3

Plot 6: PC1 against PC2 in form space (Red=f /Blue=m/ green=marked outlier) for curve 3

Curve 4

Plot 7: PC1 against PC2 in shape space (Red=f /Blue=m/ green=marked outlier) for Curve 4
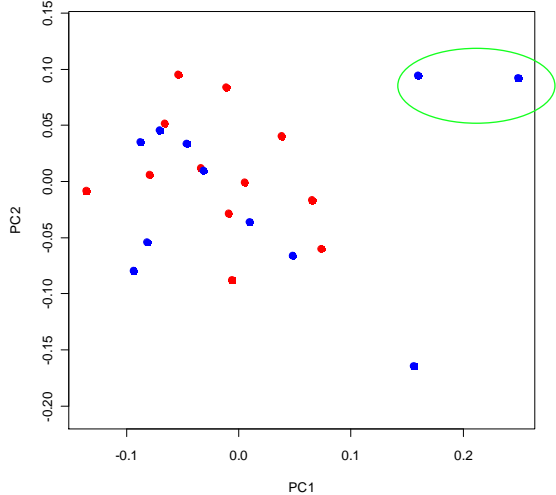
Plot 8: PC1 against PC2 in form space (Red=f /Blue=m/ green=marked outlier) for curve 4
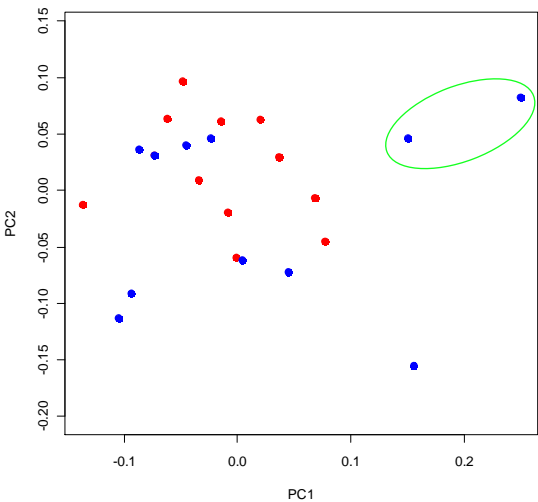
Including all specimens 45.5% and 12.2% of the variance for Curve 3 is explained by the first two partial components in shape space and 42.5% and 13.7% of the variance is explained in the first two partial components in form space. The mean differences in Curve 3 are not significant (p=0.608).

Including all specimens 27.9% und 23.3% of the variance for Curve 4 is explained by the first two partial components in shape space and 31.2% and 21.3% of the variance is explained in the first two partial components in form space. The mean differences in Curve 4 are not significant (p=0.482).

Curve 5

Plot 9: PC1 against PC2 in shape space
(Red=f /Blue=m/ green=marked outlier) for Curve 5

Plot 10: PC1 against PC2 in form space
(Red=f /Blue=m/ green=marked outlier) for curve 5

Including all specimens 36.9% and 18.8% of the variance for Curve 5 is explained to the first two partial components in shape space and 32.8% and 16.8% of the variance is explained in the first two partial components in form space. The mean differences in Curve 5 are not significant (p=0.305).

Looking for significance of the variance differences in PC1 and PC2 for each single curve was not successful.

2 Including every Curve

21 Figure shows the resulting superimposition (generalized procrustes analysis) of all used specimens (n=23, 11♂, 12♀; Caucasian, age average: 25.38 years) and all curves.

The results showed that there are no significant mean differences (permutation test/ randomized sample 999: p=0.384) in the determination of sex.

Furthermore, a principal component analysis (PCA) was implemented. Plot 11 and 12 show the first against the second principal component in shape as well as in form space. Afterwards the significance of the variance differences in PC1 and PC2 was calculated (0.87 /0.98).
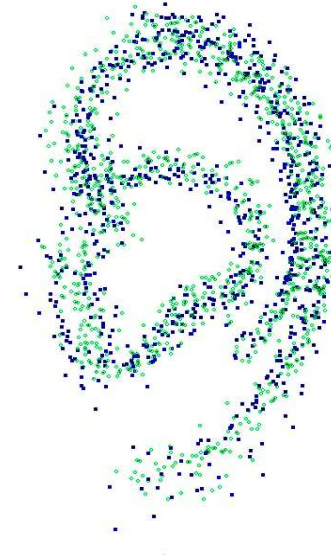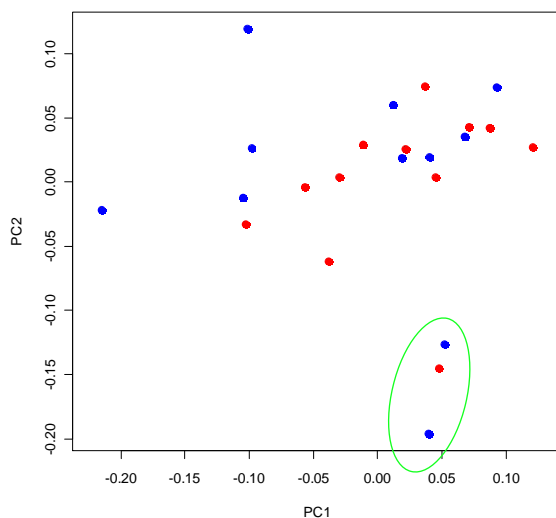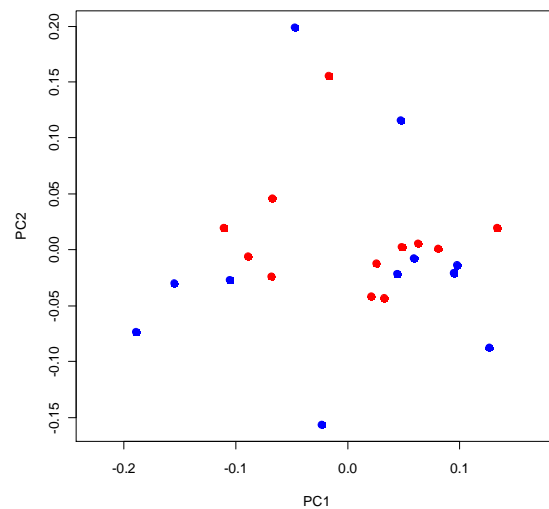

Figure: 21. Data after the GPA including used specimens (n=26, 11♂, 12♀)

Plot 11: PC1 against PC2 in shape space
(Red=f /Blue=m/ grenn=marked outlier)

Plot: 12 PC1 against PC2 in form space (Red: f / Blue: m)

Including all specimens 24.58% and 19.89% (total 44.47%) of the variance is explained to the first two partial components in shape space and 25.68% and 17.98% (total 43.66%) of the variance is explained in the first two partial components in form space (Plot 11, 12).

3   Warping the array surface

Furthermore, the array surface was warped along the first and second principal component. Figure 22a shows the warped images against the first principal component, the left image shows the mean shape including the 1st eigenvector at -0.16, the middle image the procrustes mean shape and the right side the mean shape including 1st eigenvector at +0.21.

Figure 22a: warped image (1st eigenvector -0.16)

warped image (proc.mean.shape)

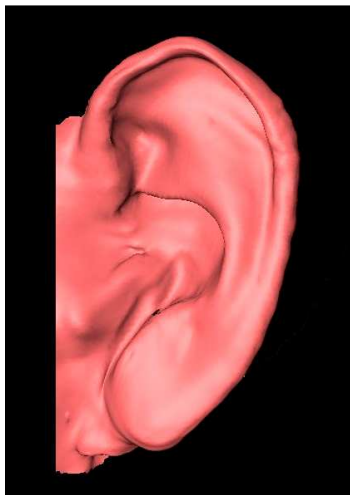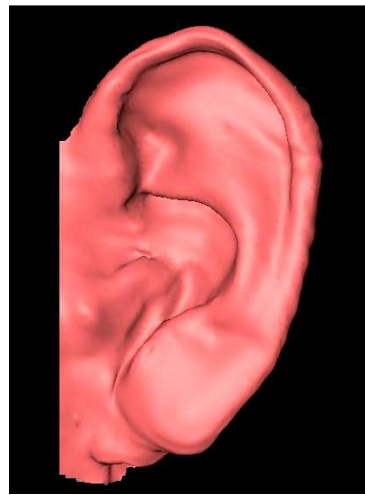warped image (1st eigenvector +0.21)

Figure 22b: : warped image (2nd eigenvector -0.16)

warped image (proc.mean.shape)

warped image (2nd eigenvector +0.21)

Figure 22b shows the warped images including the 2nd eigenvector by -0.16 (left), the procrustes mean shape (middle) and mean shape including 2nd eigenvector +0.21 (right).
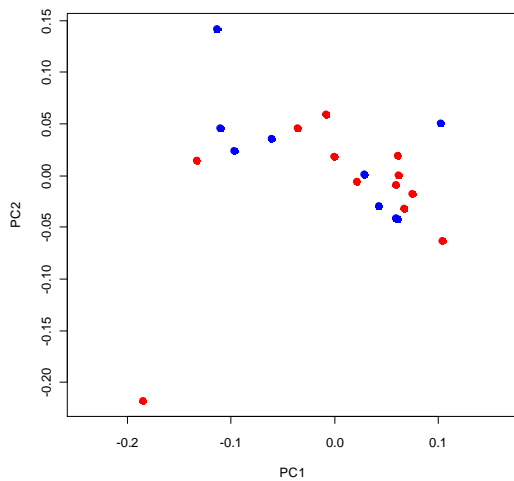
4 Excluding outliers

After excluding the two outliers (specimens 15 and 21) the data was re-examined. 28.21% and 15.69% of the variance is explained by the first two partial components (p=0.152). Looking at every curve separately in Curve 2 (Plot 13) 36.5% and 16.1% of the variance is explained by the first two partial components (p=0.518).
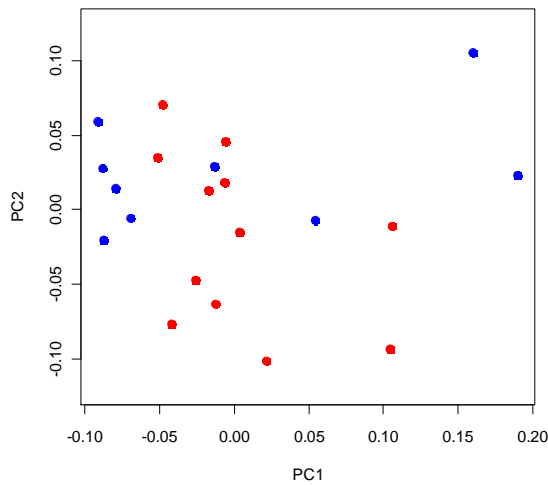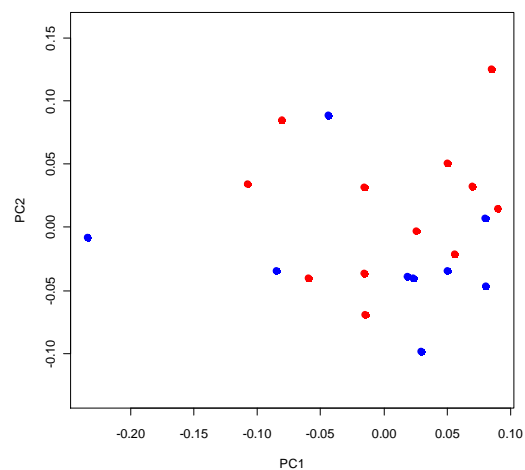

Plot 13 PC1 against PC2 in shape space (Red=f /Blue=m/ green=marked outlier) for Curve 2 excluding outliers
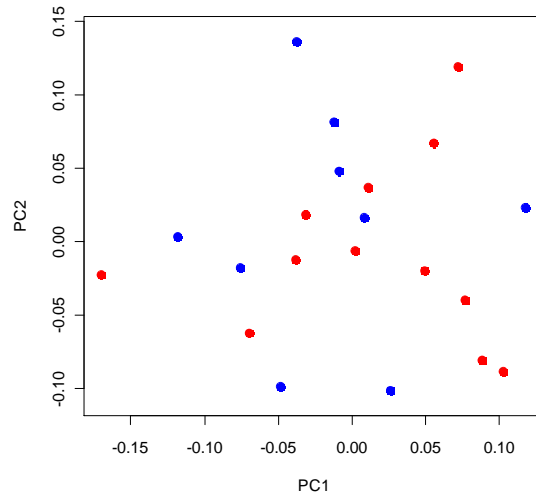
Plot 14: PC1 against PC2 in shape space (Red=f /Blue=m/ green=marked outlier) for Curve 3 excluding outliers

Plot 15 PC1 against PC2 in shape space (Red=f /Blue=m/ green=marked outlier) for Curve 4 excluding outliers

Plot 16 PC1 against PC2 in shape space (Red=f /Blue=m/ green=marked outlier) for Curve 5 excluding outliers

In Curve 3 (Plot 14) 22.8% and 18.6% of the variance is explained by the first two partial components (p=0.562). Curve 4 (Plot 15) shows 32.2% and 20.2% of the variance of the first two PC (p=0.609). In Curve 5 (Plot 16) 33.3% and 16.0% of the variance is explained by the first two partial components in shape space. The test of significance shows p=0.275. After analyzing the curves in form space similar results were visible. Moreover, no significances in the variances in PC1 or PC2 could be found.

IV. Discussion

1 Sexual Dimorphism Result

The null hypothesis states that 3D surface scans of human ears are not an appropriate method for the analysis of sexual dimorphism and therefore cannot be used in biometric recognition systems, as well as craniofacial development, human evolution or diseases. As shown in the permutation test results (p=0.384) the null hypothesis has been improved.

The results of the principal component analysis and the warped images clearly visualize where in the data the most differences between the individuals are located. The first principle component indicates that most of the differences are between the upper part of the antitragus and the space between the helix and antihelix in the antitragus region. This phenomenon could be explained with Curve 1 (Figure 16. p.17; Plot 7 p.24) which differs extremely between the individuals because of the open ending in the antitragus region. Furthermore, the angle between the crossing point of the Helix and the head is going to be more flat in Figure 22, where the mean shape including the 1st eigenvector by -0.16 is shown. So the angle between the negative and the positive value including the 1st eigenvector is steepening (Figure 22 p.27). The data along the second principle component visualize that a lot of the differences are between the upper part of the antitragus and the space between the helix and antihelix in the antitragus region too. Moreover, the whole ear is going to be more clinched along the second partial component 2 (-0.16 > proc. Mean shape > +0.21).

Looking at the separate partial component analysis of the curves it is visible that most of the changes and differences are on the first curve (see Plot 1 p.23), as well as the fourth curve (see Plot 9 p.28). On the other hand Curve 2 and 3 show almost no heavy changes, neither in both sexes (see Plot 3, p.23; 5, p.24). The plots of Curve 3, 4 and 5 show that the data has at least two outliers (marked on plot 13), while in Curve 1 and 4 these are only hardly recognizable (Plot 1 and 7).
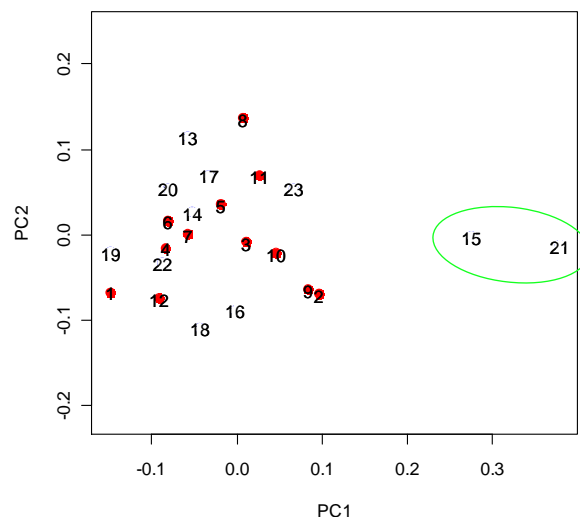
Plot 17   PC1 against PC2 in shape space (Red=f / green=marked outlier) for Curve 3 as text

30

2 Plaster mould model accuracy

The accuracy of the plaster mould model depends basically on the accuracy of the negative form, the cast composition and consistence. Laughton et al. (2002) described that plaster casting may be preferable because in general it has a low error rate. Comparison of 3D scans of human faces with scans from plaster cast of human faces using alginate, led to the result of an average deviation between 0.95 and 3.55 mm, depending on the facial region (Holberg et al., 2006). This error is based on the easy deformation of the lips, the nose and the ears during the production time of the negative form.

Sun et al. (2010) described the discrepancies of the plaster casts volume for alginate impression material as significantly ($p<0.05$) different in relations to the volume of the master models (simian dental arches), while silicone materials or impregum-penta polyether showed no significant differences.

In this diploma study the combination of alginate (as a negative form) and cast proofed to be a very convenient and adequate method, although there are limitations in the usage of these two materials that should be kept in mind. By using an adequate cast composition and consistence during the filling of the negative form, air bubbles can be prevented and the error rate of the resulting cast is therefore reduced. Including the fast processing time (within 20 minutes), after the negative alginate form was built, the error rate is limited by the easy movement of the ear during the alginate filling. The movement artifact can be reduced when the mixture is filled in the mold while the proband lies on the side. The operator can minimize this problem by first filling the part between head and ear instead of unwarily filling the mixture into the form.

3 David Laserscanner

3.1 Accuracy

The accuracy of the David Surface scanner 2.4.3 (DAVID Vision Systems GmbH, Germany), depends on various hardware components and settings, like the camera distance, the object size, the light conditions, the triangulation angle and the quality of the calibration target. Winkelbach et al. (2006) obtained an error of less than 0.4mm for the following setup: a CCD grayscale camera, a 5mW laser, two planar faces of 50.25 mm, a camera distance of about 600 mm, and a triangulation angle of approximately 30°-35°. The David Surface scanner 2.4.3 manufacturer describes a general error of not more than 1% of the camera distance (DAVID 3D Scanner: Jan 2011)

Having two images, overlapping 35% and starting to fuse them, Winkelbach et al. (2006) described after 0.5 seconds that 50 % already achieved a rotational accuracy of less than 2°.

It appears that the resulting *.obj surfaces showed degenerated triangles with a zero point area, which had to be removed first, before further steps in the analysis could be made.

In this diploma study a maximum error of not more than 3mm per scan can be expected, because of a camera distance of 300 mm. Moreover, a maximum error of 2° during the shape fusion for every scan can be expected. Based on this data, it is likely that the rotational error can be higher because every 3D image is the result of 4-6 single scans.

3.2 Quality

The scan quality can be affected by several facts, namely the camera and laser quality or the calibration corner. To obtain better results, the digital camera should have as little noise as possible, a high photosensitivity or should be a simple grayscale camera instead of a color camera where most color pixels are interpolated. Additionally, the laser line should be as thin and as bright as possible and the calibration corner must have an exact angle of 90° (DAVID 3D Scanner: Jan 2011).

Because the scans were made by moving the laser manually the camera settings and the image format had to be changed. Since the original settings for the scanner would include a resolution of 1600*1200 pixels and a frame rate of 12 pictures per second the scan of the ear would take 100 seconds (1200 frames to get all lines filled). Therefore, a resolution of 640*480 pixels and a frame rate of 30 pictures per second had been chosen, resulting a total scanning time of 16 seconds per image. With these settings the movement artifacts can be reduced and the interpolation rate, the smooth average and the smooth median can be set down (DAVID 3D Scanner: Jan 2011).

To get an accurate result regarding the accuracy or potential of the David Laserscanner for complex structures it would be important to get a second set of scans from a different 3D Laserscanner. Therefore, a fully functional 3D Laserscanner, with known error possibilities would be obligatory.

After pretests using the Breuckmann OptoTop HE Laserscanner (Breuckmann GmbH, Germany) at the Department of Anthropology (University of Vienna, Austria) it has been shown that because of the heavy movement of the subject, a lot of scans
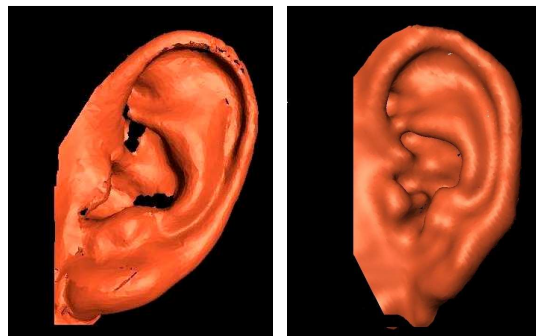

Figure23a: Results of pretested Breuckmannscans

Figure 23b: Resulting shape fusion of 10 single scans

would be necessary plus a fixation of the head has to be provided. However, resulting from the longer exposure time more artifacts emerge. Chang et al. (2003) considered a potential measurement error depending on exposure time, light arrangements, shadowing and occlusion. These problems in imaging the auricle, which has a hardly ascertainable three dimensional structure led to disaffecting results (see Figure 23a) and inappropriate shape fusion results (see Figure 23b) obtained by the Breuckmann optotop Laserscanner (Breuckmann GmbH, Germany) at the Department of Anthropology, (University of Vienna, Austria).

4 Digitizing of 72 landmarks including 67 semilandmarks

In total 23 specimens (Caucasian, 11♂, 12♀; age average: 25.4) were included in the statistical data analysis, six specimens were excluded from the study due to missing data in the 3D surfaces.

All 72 landmarks including 67 semilandmarks were set by the same observer along specific visible curves (parabolic and ridge curves) of the surface structure, 4 of the curves open and 1 of them closed (see Figure 24).

The resolution property of the bare human eye amounts under ideal conditions about 0.5mm. Furthermore it can reach under good contrast 0.3mm (Lange and Benning, 2006). Consequently at the 3D data digitization continues quality could not precisely be insured by handling the data only with Amira 5.2.0 (Visage Imaging Inc., San Diego, USA) at the Department of Oral Surgery (Medical University of Vienna, Austria). So cross sections in Edgewarp 3.30 (Bookstein and Green, 2006) were used to ensure the accuracy of digitizing semilandmarks at characterized cubic-parabolic and ridge curves (Figure 16) and landmark on extreme point (Figure 15; p.17).
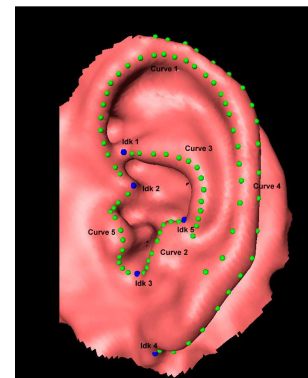

Figure 24: digitizing of 72 landmarks including 67 semilandmarks

V. Conclusion

This diploma study tried to verify that 3D surface scans of human ears are an appropriate method for the analysis of sexual dimorphism, which can be used in biometric recognition systems, as well as craniofacial development, human evolution or diseases.

Concerning sex specific differences in the determination of sexual dimorphism of human ears, analyzing 3D image data from the David Laserscanner 2.4.3 (DAVID Vision Systems GmbH, Germany) showed no significant differences after a p-test MANOVA. The analysis with geometric morphometrics although seems to be an appropriate method for analyzing three dimensional surface scan data obtained from the David Laser scanner 2.4.3 (DAVID Vision Systems GmbH, Germany).

The reduced sample size of 23 specimens does not allow an accurate prediction of sexual dimorphism of human ears. The first principle component indicates that most of the individual differences are between the upper part of the antitragus and the space between the helix and antihelix in the antitragus region. This phenomenon could be explained with Curve 1 (Figure: 16, p. 17; Plot 9 p.25) which differs between the individuals extremely, because of the open ending in the antitragus region. Similar results can be found in the second principle component.

The usage of the plaster mould model has showed very good accuracy in comparison to the actual ears geometry. Therefore, adequate preparation (mixture of alginate) and trained handling (filling of mould) is important to get optimal results.

The accuracy of the David Surface scanner 2.4.3 (DAVID Vision Systems GmbH, Germany), depends on various hardware components and settings, like the camera distance, the object size, the light conditions, the triangulation angle and the quality of the calibration target. In this study a maximum error of not more than 3mm per scan can be expected, because of a camera distance of 300 mm. By using a stepper motor (currently under construction by the author) instead of manual handling of the laser, movement artifacts could be reduced and a higher image resolution could definitely improve the data quality. Additionally, for complex structures it would be important to get a second set of scans from a different 3D Laserscanner with known error possibilities.

In general, it could be shown that there is a limited potential of the David Laser scanner 2.4.3 (as an example for 3D surface scanners) for the analysis of complex structures like human ears.

VI. Appendix

List of Abbreviations:

GPA .... Generalized procrustes analysis

PCA ....Principal Component Analysis

ICP ....Iterated closest point

LM ....landmark

SLM ....semilandmarks

SNAKES ....Sliding landmarks

MANOVA .... Multivariate analysis of variance

PC ....principal component

PROC .... procrustes

*.obj .... Relocatable Object Module Format

*.stl ....Stereolithography CAD native file format

*.cur .... Cursor graphics file format

*.sav ....Executable/ Backup file format

*.sur ....Surface file format

*.mtl .... Wavefront, Morphologika file format

*.xls ....Exel file format

*.Ascii ....American Standard Code for Information Interchange

List of Figures:

„Ich habe mich bemüht, sämtliche Inhaber der Bildrechte ausfindig zu machen und ihre Zustimmung zur Verwendung der Bilder in dieser Arbeit eingeholt. Sollte dennoch eine Urheberrechtsverletzung bekannt werden, ersuche ich um Meldung bei mir."

List of Plots

Software used: R.1.12.1: (R-Project: Institute of Mathematic, WU Vienna) 2010

Plot 1: PC1 against PC2 in shape space (Red=f /Blue=m/ green=marked outlier) for Curve 1

Plot 2: PC1 against PC2 in form space (Red=f /Blue=m/ green=marked outlier) for Curve 1

Plot 3: PC1 against PC2 in shape space (Red=f /Blue=m/ green=marked outlier) for Curve 2

Plot 4: PC1 against PC2 in form space (Red=f /Blue=m/ green=marked outlier) for Curve 2

Plot 5: PC1 against PC2 in shape space (Red=f /Blue=m/ green=marked outlier) for Curve 3

Plot 6: PC1 against PC2 in form space (Red=f /Blue=m/ green=marked outlier) for Curve 3

Plot 7: PC1 against PC2 in shape space (Red=f /Blue=m/ green=marked outlier) for Curve 4

Plot 8: PC1 against PC2 in form space (Red=f /Blue=m/ green=marked outlier) for Curve 4

Plot 9: PC1 against PC2 in shape space (Red=f /Blue=m/ green=marked outlier) for Curve 5

Plot 10: PC1 against PC2 in form space (Red=f /Blue=m/ green=marked outlier) for Curve 5

Plot 11: PC1 against PC2 in shape space (Red=f /Blue=m/ green=marked outlier)

Plot 12: PC1 against PC2 in form space (Red=f /Blue=m/ green=marked outlier)

Plot 13: PC1 against PC2 in shape space (Red=f /Blue=m/ green=marked outlier) for Curve 2 excluding outliers

List of Tables

List of Equations:

Software References

Licensed:

(1)   David Laserscanner 2.4.3 (DAVID Vision Systems GmbH, Germany) at the Department of Anthropology, University of Vienna, Austria

(2)   Visage Imaging Amira 5.2.0 (Visage Imaging Inc., San Diego, USA) at the Department of Oral Surgery, Medical University of Vienna, Austria

(3)   Breuckmann opto Top HE (Breuckmann GmbH, Germany) at the Department of Anthropology, University of Vienna, Austria

Open source:

(1)   Edgewarp3.30 (Bookstein, Green 2006)

(2)   Morpheus et al. Software for morphometric research. Revision 01-31-00, Department of ecology and evolution, State University of NY at Stony Brook, NY (Slice 2007)

(3)   MeshLab V 1.2.1 (Istituto di Scienza e Tecnologie dell'Informazione/ Stable Developer: Callieri, Corsini, Dellepiane, Ganovelli, Pietroni, Tarini) open sauce since 2007

(4)   R.1.12.1: (R-Project: Institute of Mathematic, School of Economy, Vienna) 2010

References

(1)   Adams, Rohlf, Slice (2004): Geometric morphometrics: ten years of progress following the'revolution'. Italian Journal of Zoology, 71(1):5$^{\perp}$ 16, 2004.

(2)   Arbab-Zavar and Nixon (2007): On shape-mediated enrolment in ear biometrics. International Symposium on Visual Computing (ISVC), 26-28 November 2007, Nevada

(3)   Bastir, Rosas, O'Higgins (2006): Craniofacial levels and the morphological maturation of the human skull, *J. Anat.* 209 (2006), pp. 637–645

(4)   Bhanu and Chen (2003): Human ear recognition in 3D. Workshop on Multimodal User Authentication, pages 91–98, 2003

(5)   Bertillon (1890): La photographie judiciaire, avec un appendice sur la classification et l'identification anthropometriques. Gauthier-Villars, Paris, 1890.

(6)   Bookstein (1989): Principal warps: thine-plate slines and de decomposition of deformation. IEEE Transaction on pattern analysis and machine intelligens 11:567-585

(7)   Bookstein (1991): Morphometrics tools for landmarks data: Geometry and Biology. Cambridge University Press

(8)   Bookstein (1996): F.L. Bookstein, Applying landmark methods to biological outline data. In: K.V. Mardia, C.A. Gill and I.L. Dryden, Editors, *Image Fusion and Shape Variability Techniques*, Leeds University Press, Leeds (1996).

(9)   Bookstein (1997): landmark methods for form without landmarks: mophometrics of group differences in outline shape, *Med. Image Anal.* 1 (1997), pp. 225–243.

(10)   Bookstein, Schäfer, Prossinger, Seidler, Fieder, Stringer, Weber, Arsuaga, Slice, F.J. Rohlf, Recheis, Mariam and Marcus (1999): Comparing frontal cranial profiles in archaic and modern Homo by morphometric analysis, *Anat. Rec. (New Anat.)* 257 (1999), pp. 217–224.

(11)   Bookstein (1999b): Linear methods for nonlinear maps: Procrustes fit, thin-plate splines, and the biometric analysis of shape variability. In: A Toga (ed.) Brain Warping. London: Academiv press, pp 157- 181

(12)   Bookstein et al. (2002): F.L. Bookstein, P.D. Sampson, P.D. Connor and A.P. Streissguth, Midline corpus callosum is a neuroanatomical focus of fetal alcohol damage, *Anat. Rec. (New Anat.)* 269 (2002), pp. 162–174.

(13)   Bookstein et al. (2003): F.L. Bookstein, P. Gunz, P. Mitteroecker, H. Prossinger, K. Schaefer and H. Seidler, Cranial integration in Homo: singular warp analysis of the midsagittal plane in ontogeny and evolution, *J. Hum. Evol.* 44 (2003), pp. 167–187.

(14) Bookstein, Schaefer, Mitteroecker, Gunz, Seidler (2004): The geometry of anthropometrics: A new typology of landmarks. Am. J. Phys. Anthropol., Suppl. 38, 66.

(15) Burge and Burger (1998): Ear Biometrics. In A. Jain R. Bolle and S. Pankanti, editors, BIOMETRICS: Personal Identification in a Networked Society, pp. 273-286. Kluwer Academic, 1998.

(16) Burge and Burger (2000): Ear Biometrics in Computer Vision. In the 15th International Conference of Pattern Recognition, ICPR 2000, pp. 826-830.

(17) Carlbom, Paciorek (1978): Planar Geometric Projections and Viewing Transformations Computing Survery, Vol.10, No.4, Dezember 1978 pp.463-502

(18) Chang, Bowyer, Sarkar, Victor (2003): Comparison and Combination of Ear and Face Images in Appearance-Based Biometrics. IEEE Transactions on Pattern Analysis and Machine Intelligence, vol. 25, no. 9, September 2003, pp. 1160-1165

(19) Chen and Bhanu (2004): Human ear detection from side face range images. International Conference on Pattern Recognition, pages 574–577, 2004.

(20) Chen and Bhanu (2005): Contour matching for 3D ear recognition. Seventh IEEE Workshop on Application of Computer Vision, pages 123–128, 2005.

(21) DAVID 3D Scanner: http://www.david-Laserscanner.com/wiki/user_manual (Jan.2011)

(22) Dirichlet (1859): "Über die Reduktion der positiven quadratischen Formen mit drei unbestimmten ganzen Zahlen," J. Reine Angew. Math., vol. 40, pp. 209-227, 1850

(23) Dryden and Mardia (1998): Statistical shape analysis. NY: John Wiley and Sons

(24) EVAN (2010): University of Vienna; Virtual anthropology http://www.virtual-anthropology.com/virtual-anthropology/geometric-morphometrics/procrustes-superimposition (25.June.2010)

(25) Fisher (1918): The Correlation Between Relatives on the Supposition of Mendelian Inheritance, *Philosophical Transactions of the Royal Society of Edinburgh* in 1918, (volume 52, pages 399–433)

(26) Fisher (1921): On the "Probable Error" of a Coefficient of Correlation Deduced from a Small Sample.Metron 1921,1,1-32

(27) Foucar (1940): Congenital abnormalities of the external ear; Can Med Assoc J. 1940 July; 43(1): 26–27

(28) Gower (1975): Generalized Procrustes Analysis, Psychometrica 40: 33-51

(29) Gunz et al. (2005): Gunz, Mitteroecker and Bookstein, semilandmarks in three dimensions. In: D. Slice, Editor, *Modern Morphometrics in Physical Anthropology*, Kluwer Academic/Plenum Publishers, New York (2005), pp. 73–98

(30) Holberg , Schwenzer , Mahaini , Rudzki-Janson (2006): Accuracy of facial plaster casts; Angle Orthodontist 2006 Jul; 76(4):605-11. Gemany, Munich

(31) Hotelling (1933): Analysis of a complex of statistical variables into principal components. Journal of educational Psychology 24:417

(32) Hurley, Nixon, Carter (2000): A NEW FORCE FIELD TRANSFORM FOR EAR AND FACE RECOGNITION. In: Proceedings of the IEEE 2000 International Conference on Image Processing ICIP2000. pp. 25-28.

(33) Hurley, Nixon, Carter (2005): Force field feature extraction for ear biometrics, Computer Vision and Image Understanding, v.98 n.3, p.491-512, June 2005

(34) Hurley, Arbab-Zavar and Nixon (2007): THE EAR AS A BIOMETRIC. In: EUSIPCO 2007, 2007, Poznan, Poland. pp. 25-29.

(35) Iannarelli (1989): Ear identification. Forensic identification series. Paramount publishing company, Fremont, California

(36) Jain, Flynn and Ross (2007): Handbook of Biometrics, Springer, Forthcoming 2007. Messer, Matas, Kittler, Luettin, and Maitre.(1999) Xm2vtsdb: The extended m2vts database. In Proc. AVBPA, Washington D.C., 1999.

(37) Kahle und Frotscher (2005): (eds) 9 Auflage, Taschenatlas Anatomie in 3 Bänden; 3 Nervensystem und Sinnesorgane Georg Thieme Verlag pp.366 ff.

(38) Katina S, Bookstein FL, Gunz P, Schaefer K, (2007): Was it worth digitizing all those curves? A worked examplefrom craniofacial primatology. : AJPA, AAPA Abstract, S44: 140

(39) Kendall (1984): Shape-manifolds, Procrustean metrics and complex projective spaces, Bulletin of the London Mathematical Society 16:81-121

(40) Kendall (1985): Exact distributions for shapes of random triangles in convex sets, Advan. Appl. Prob. 17:308-329

(41) Kenneth (2000): Point and Vector. Computer Science Department, University of California   http://cmp.felk.cvut.cz/cmp/courses/pvi2003/LectureNotesPVI2003/Points-and-Vectors.pdf (1.June 2010)

(42) Klingenberg (2004): Integration, modules and development: molecules to mophology to evolution. In Pigliucci, K. and Preston, K. editors. Phenotypie integration: studying the ecology and evolution of complex phenotypes. New York: Oxford University Press

(43) Klingenberg (2009): 50111 Analysis of organismal form: An introduction to morphometrics, delivered as a Web-based course University of Manchester UK2009

(44) Koenderink (1990): The Solid Shape; The MIT Press, Cambridge, Massachusetts, London, England; Chapter 6.7.5 pp.297-303

(45) Kucera and Malmgren (1996): Latitudinal variation in the planktic foraminifera Contusatruncana contusa in the terminal Cretaceous ocean. Marine Micropaleontology 28:31–52.

(46) Lange and Benning (2006): Verfahren zur Rissanalyse bei Betonbauteilen; DGZfP-Berichtsband 100-CD; Fachtagung Bauwerksdiagnose: Praktische Anwendungen Zerstörungsfreier Prüfungen, Berlin

(47) Lanman and Taubin, (2009): Build your own 3D Scanner. 3D Photography for beginners; Siggraph 2009: ACM SIGGRAPH 2009 courses (eds.) 2009 ACM New York.

(48) Laughton, McClay Davis, Williams (2002): A Comparison of Four Methods of Obtaining a Negative Impression of the Foot; Journal of the American Podiatric Medical Association Volume 92 Number 5 261-268 2002

(49) Lauter et al. (2000): Mathematik Sekundarstufe II Analytische Geometrie und Liniare Algebra. Erweiterte Ausgabe. Cornelsen

(50) Lohmann (1983): Eigenshape analysis of microfossils: A general morphometric method for describing changes in shape. Mathematical Geology 15:659-672.

(51) Lohmann and Schweitzer (1990a): *Globorotalia truncatulinoides'* growth and chemistry as probes of the past thermocline: 1: shell size. Paleoceanography 5:55–75.

(52) Lohmann and Schweizer (1990b): On eigenshape analysis. Pp. 145-166 in Rohlf, F. J. and Bookstein, F. L., eds. Proceedings of the Michigan Morphometrics Workshop. The University of Michigan Museum of Zoology, Special Publication P. N. No. 2, Ann Arbor

(53) Lüllmann-Rauch (2006): (eds.) 2.Auflage, Taschenlehrbuch: Histologie; Georg Thieme Verlag pp.553 ff.

(54) MacLeod and Carr (1987): Morphometrics and the analysis of shape in conodonts. Pp. 168–187 in Austin, R. L., eds. Conodonts: Investigative Techniques and Applications. Ellis Horwood Limited, Chichester.

(55) MacLeod and Rose (1993): Inferring locomotor behavior in Paleogene mammals via eigenshape analysis. American Journal of Science 293-A:300-355.

(56) MacLeod (1999): Generalizing and extending the eigenshape method of shape space visualization and analysis/ Paleobiology 25(1), 1999, pp. 107-138

(57) Meijerman, van der Lugt, Maat (2007): Cross-sectional anthropometric study of the external ear. Barge's Anthropologica, Deptartment of Anatomy, Leiden University Medical Center; J Forensic Sci. 2007 Mar;52(2):286-93.

(58) Messer, Matas, Kittler, Leuttin, Maitre (1999): XM2VTSDB: the extended M2VTS Database, Proc. AVBPA´99 Washington DC

(59) Mitteroecker et al. (2004): P. Mitteroecker, P. Gunz, M. Bernhard, K. Schaefer and F.L. Bookstein, Comparison of cranial ontogenetic trajectories among great apes and humans, *J. Hum. Evol.* 46 **(**2004), pp. 679–698.

(60) Mitteroecker et al., (2005): P. Mitteroecker, P. Gunz and F.L. Bookstein, Heterochrony and geometric morphometrics: a comparison of cranial growth in *Pan paniscus* versus *Pan troglodytes*, *Evol. Dev.* **7** (2005), pp. 244–258

(61) Mitteröcker and Gunz (2009): Advances in Geometric Morphometrics, Advanced Imaging in Biology and medicine- Technology, Software, Enviroments, Applications. Hallgrimsson, Sense (eds.) Heidelberg; Springer 2009

(62) Moreno, Sánchez, Vélez. (1999): On the Use of Outer Ear Images for Personal Identification in Security Applications. IEEE 33rd Annual International Carnahan Conference on Security Technology, 1999, pp. 469-476.

(63) Niemitz, Nibbrig, Zacher (2007): Human ears grow throughout the entire lifetime according to complicated and sexually dimorphic patterns--conclusions from a cross-sectional analysis. Anthropol Anz. 2007 Dec;65(4):391-413.

(64) Norris, Corfield and Cartlidge (1996): What is gradualism? Cryptic speciation in globorotaliid foraminifera. Paleobiology 22:386–405

(65) Pearson (1895): Note on regression and inheritance in the case of two parents. Proceeding of the Royal Society of London 58:240-242

(66) Pearson (1901): On lines and planes of closest fit to system of points in space. Phil Mag Ser 6:559:572

(67) Peeples, Dixon, Buss (1985): Genetic analysis of the pinna of the human ear: sex differences in college age adults; JHered (1985) 76 (5): 390-392

(68) Purkait and Singh (2008): "A test of individuality of human external ear pattern: Itsapplication in the field of personal identification" Forensic Science International 178 (2008) 112–118

(69) Ray (1990): Application of eigenshape analysis to second order leaf shape ontogeny in Syngonium podophyllum (Araceae). Pp. 201–213 in Rohlf, F. J. and Bookstein, F. L., eds. Proceedings of the Michigan Morphometrics Workshop. The University of Michigan Museum of Zoology, Special Publication 2, Ann Arbor, MI

(70) Rohlf and Slice (1990): Extensions of the Procrustes method for the optimal superimposition of landmarks, Systematic Zoology 39: 40-59

(71) Rohlf (1998): On Applications of Geometric Morphometrics to Studies of Ontogeny and Phylogeny. *Systematic Biology*.

(72) Sadler and Langman (2003): Medizinische Embryologie: die normale menschliche Entwicklung und ihre Fehlbildungen; Thieme Verlag; Chapter 17

(73) Sheets et al. (2004): D.H. Sheets, K. Kim and C.E. Mitchel, A combined landmark and outline-based approach to ontogenetic shape change in the Ordovician trilobite *Triarthrus becki*. In: A. Elewa, Editor, *Morphometrics. Applications in Biology and Paleontology*, Springer-Verlag, Berlin Heidelberg (2004), pp. 67–82.

(74) Sforza, Grandi, Binelli, Tommasi, Rosati and Ferrario (2009): Age- and sex-related changes in the normal human ear; Forensic Science International 187 (2009) 110.e1– 110.e7 pp

(75) Slice, Rohlf, Bookstein, Marcus (1995): Glossary for Geometric Morphometrics; http://life.bio.sunysb.edu/morph/glossary/gloss1.html (Jan.2010)

(76) Slice (1998): Morpheus et al.: Software for morphometric research. Revision 01-31-00, Department of ecology and evolution, State University of NY at Stony Brook, NY

(77) Slice (2005): Modern Morphometrics in physical anthropology: eds 2005; Kluwer Academic/ Plenum Publisher NY

(78) Sun, Li, Chu (2010): Three-dimensional accuracy of plaster casts obtained using three impression materials; Nan Fang Yi Ke Da Xue Xue Bao. 2010 Feb; 30(2):257-9. Chinese

(79) Thompson (1917): On growth and Form; Cambridge university Press

(80) Victor, Bowyer, Sarkar (2002): An evaluation of face and ear biometrics in Proceedings of International Conference on Pattern Recognition, pp. 429-432, August 2002.

(81) Weber and Bookstein (2011): Virtual Anthropology: A Guide to a new interdisciplinary field, Springer Wien NewYork 1st Edition

(82) Winkelbach, Molkenstruck, Wahl (2006): Low-Cost Laser Range Scanner and Fast surface Registration Approach; Institut for Robotic and process control; In Franke et al. (Eds.) DAGM, LNCS 2006, Volume 4174, 718-728, DOI: 10.1007/11861898_72

(83) Wright (1997): Development of the human external ear J Am Acad Audiol. 1997 Dec;8(6):379-82; Callier Center for Communication Disorders, University of Texas at Dallas, USA 1997

(84) Yan and Bowyer (2004): 2D and 3D ear recognition. In Biometric Consortium Conference, 2004.

(85) Yan and Bowyer (2005a): ICP-based approaches for 3d ear recognition. In Biometric Technology for Human Identification II, Proc. of SPIE, volume 5779, pages 282-291, 2005.

(86) Yan and Bowyer (2005b): A fast algorithm for ICP-based 3d shape biometrics. In Fourth IEEE Workshop on Automatic Identification Advanced Technologies (AutoID), pages 213-218, NY, 2005

(87) Yan and Bowyer (2005c): Empirical evaluation of advanced ear biometrics. In IEEE Computer Society Conference on Computer Vision and Pattern Recognition (CVPR'05) - Workshops, page 41, 2005.

(88) Yan and Bowyer (2007): Biometric recognition using three-dimensional ear shape. IEEE Trans. Pattern Analysis and Machine Intelligence. Volume 29 , Issue 8 pp:1297-1308

Einverständniserklärung:

Hiermit erkläre ich mich einverstanden, dass meine Daten zu wissenschaftlichen Zwecken verwendet werden und ich zu keinem späteren Zeitpunkt dieses Einverständnis zurückziehen kann.

Es handelt sich um die Verwendung von Ohrmodellen des linken Ohres in Form von Alginat- und Gipsabdrücken.

Diese Modelle werden in weiter Folge unter Berücksichtigung spezifischer Fragestellungen untersucht.

_____
Datum, Unterschrift des teilnehmenden Probanden

_____
Unterschrift des Versuchsleiters

CURRICULUM VITAE

PERSONAL INFORMATION

Name:	Katharina Baron
Date of birth:	10 September 1985; Hildesheim, Germany
E-mail:	Katharina.Baron@gmail.com

EDUCATION

Oct 10 – April 11	Diploma thesis:
	Morphometric shape analysis of human ears: approaches via 3d surface-scans of plaster mould models of living individuals in the determination of sex
Oct 06 – April 11	University of Vienna, (Austria); A442 Physical Anthropology, Geometric Morphometrics (Mag rer nat. program)
Dec 08– April 11	Medical University of Vienna: Medicine (Co-registration)
Aug 02 – Jun 06	A-levels (Abitur)
	Graf- Anthon-Günther-Gymnasium; (Oldenburg, Germany)

WORKING EXPERIENCE

Dec 08 –	Research assistant at the 'Ludwig-Boltzmann-Institute for experimental and clinical traumatology' (Austrian Cluster for tissue regeneration) (Vienna, Austria)

SCIENTIFIC ACTIVITIES:

Publications

Sandholzer M, **Baron K,** Heimel P, Dobsak A, Metscher B

MICRO-CT ANALYSIS OF HEAT-INDUCED CHANGES IN HUMAN MOLARS AFTER EXPOSURE TO CONTROLLED THERMAL STRESS

Forensic Science International (Under Review 2011)

Ulrike Kuchler, Tina Spilka, **Katharina Baron**, Stefan Tangl, Georg Watzek, Reinhard Gruber

INTERMITTENT PTH FAILS TO STIMULATE OSSEOINTEGRATION IN DIABETIC RATS

Clinical Oral Implants Research" 2011

Posters

Baron K, Sandholzer M, Metscher B

MICRO-CT ANALYSIS OF ADULT HUMAN MOLARS AND PREMOLARS BEFORE AND AFTER EXPOSURE TO CONTROLLED HIGH TEMPERATURES

Vth International Anthropological Congress of Ales Hrdlicka, Prague (Czech Republic), 2.Sep-5.Sep.09

Sandholzer M, **Baron K**, Metscher B

MICRO-CT ANALYSIS OF HUMAN MOLARS BEFORE AND AFTER EXPOSURE TO CONTROLLED THERMAL STRESS

4th Meeting of Junior Scientists in Anthropology, Freiburg im Breisgau (Germany) 25.March.-28.March.10

Conference presentations (as Co-Author)

Sandholzer M, **Baron K**, Heimel P, Metscher B

MICRO-CT EVALUATION OF HEAT-INDUCED ALTERATIONS IN HUMAN TEETH

12th Annual BABAO Conference, University of Cambridge (United Kingdom) 17.9-19.9.2010

ADDITIONAL QUALIFICATIONS

Language skills: German (Mother tongue); English (excellent)

Technical skills: X-ray apparatus; Micro-CT; 3D Surface-scanner, Photomodeler

Computer skills: Personal And Macintosh Computer; Linux, MsOffice, OpenOffice, SPSS, R, Mathematica, Macromedia Dreamweaver CS4, HTML; Adope Photoshop, 2D and 3D visualization Software: Visage Imaging Amira; MorphoJ; Edgewarp3.30 (Bookstein, Green 2006); Morpheus et al (Slice); tps (Rohlf); Rapidform,

ADDITIONAL ACTIVITIES

Oct 06 – Jun.11   STUDENT COUNSELOR *(Austrian National Union of Students)*

Oct 09 - Jun 11   Student Counselor *(Austrian National Union of Students)* MEMBER AND DEPUTY CHAIRMAN OF BIOLOGY at the University of Vienna.

Feb 08   28. SPURENWORKSHOP OF THE GERMAN SOCIETY OF LEGAL MEDICINE; *Austria, Salzburg*

May 09   XXI CONGRESS OF THE INTERNATIONAL ACADEMY OF LEGAL MEDICINE; *Portugal, Lisbon*

Sep 09   VTH INTERNATIONAL ANTHROPOLOGICAL CONGRESS OF ALEŠ HRDLIČKA *Czech Republic, Prague*

Nov 09 – Jan 10   ANALYSES OF ORGANISMAL FORM: An introduction to morphometrics, delivered as a Web-based course; *England, University of Manchester*

March 10   EUROPEAN CONGRESS OF RADIOLOGY**,** *Austria, Vienna*

March 10   4TH MEETING OF JUNIOR SCIENTISTS IN ANTHROPOLOGY, *Germany**,** Freiburg im Breisgau*

March 11   EUROPEAN CONGRESS OF RADIOLOGY, *Austria, Vienna*